

1
2
3
4
5
6
7
8
9
10
11
12
13
14
15
16
17
18
19
20
21
22
23
24
25
26
27
28
29
30
31

Development and Evaluation of the Aerosol Forecast Member in NCEP's Global Ensemble Forecast System (GEFS-Aerosols v1)

Li Zhang^{1,2}, Raffaele Montuoro^{1,2}, Stuart A. McKeen^{1,3}, Barry Baker^{4,5}, Partha S. Bhattacharjee⁶, Georg A. Grell², Judy Henderson², Li Pan⁶, Gregory J. Frost³, Jeff McQueen⁷, Rick Saylor⁸, Haiqin Li^{1,2}, Ravan Ahmadov^{1,2}, Jun Wang⁷, Ivanka Stajner⁷, Shobha Kondragunta⁹, Xiaoyang Zhang¹⁰, Fangjun Li¹⁰

¹CIRES, University of Colorado, Boulder, CO, US;

²Global Systems Laboratory, Earth System Research Laboratory, NOAA, Boulder, CO, US;

³Chemical Sciences Laboratory, Earth System Research Laboratory, NOAA, Boulder, CO, US;

⁴NOAA Air Resources Laboratory, College Park, MD, US;

⁵Cooperative Institute for Climate and Satellites, University of Maryland, College Park, MD, US;

⁶J.M. Systems Group at NCEP/NWS/EMC, College Park, MD, US;

⁷Environmental Modeling Center, National Weather Service, Greenbelt, MD, US;

⁸NOAA Air Resources Laboratory, Oak Ridge, TN, US;

⁹NOAA/NESDIS Center for Satellite Applications and Research, Greenbelt, MD, US;

¹⁰Department of Geography, South Dakota State University, Brookings, SD, US

Submit to Geoscientific Model Development

May 2022

Deleted: March

*Correspondence to: Li Zhang (kate.zhang@noaa.gov)

CIRES, University of Colorado Boulder

GSL EPAD, NOAA ESRL

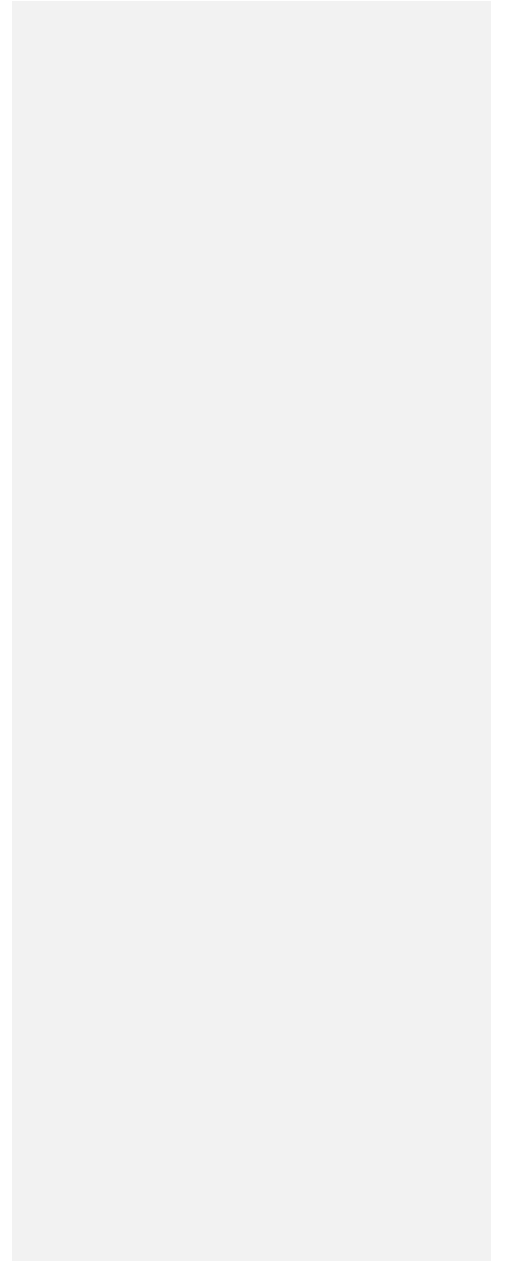
325 Broadway David Skaggs Research Center R/GSL1

Boulder, CO 80305

1-303-497-3956

1

2



1 **Abstract.**

2 NOAA's National Weather Service (NWS) is on its way to deploy various operational prediction applications using the Unified
3 Forecast System (<https://ufsccommunity.org/>), a community-based coupled, comprehensive Earth modeling system. An aerosol
4 model component developed in a collaboration between the Global Systems Laboratory, Chemical Science Laboratory, the
5 Air Resources Laboratory, and Environmental Modeling Center (GSL, CSL, ARL, EMC) was coupled online with the
6 FV3 Global Forecast System (FV3GFS) using the National Unified Operational Prediction Capability (NUOPC)-based NOAA
7 Environmental Modeling System (NEMS) software framework. This aerosol prediction system replaced the NEMS GFS
8 Aerosol Component [version 2 \(NGACv2\)](#) system in the National Center for Environment Prediction (NCEP) production suite
9 in September 2020 as one of the ensemble members of the Global Ensemble Forecast System (GEFS), dubbed GEFS-Aerosols
10 v1. The aerosol component of atmospheric composition in GEFS is based on the Weather Research and Forecasting model
11 (WRF-Chem). GEFS-Aerosols includes bulk modules from the Goddard Chemistry Aerosol Radiation and Transport model
12 (GOCART). Additionally, the biomass burning plume rise module from High-Resolution Rapid Refresh (HRRR)-Smoke
13 based on WRF-Chem was implemented; the GOCART dust scheme was replaced by the FENGSHA dust scheme (developed
14 by ARL); the Blended Global Biomass Burning Emissions Product (GBBEPx version 3) provides biomass burning emission
15 and Fire Radiative Power (FRP) data; and the global anthropogenic emission inventories are derived from the Community
16 Emissions Data System (CEDS). All sub-grid scale transport and deposition is handled inside the atmospheric physics routines,
17 which required consistent implementation of positive definite tracer transport and wet scavenging in the physics
18 parameterizations used by NCEP's operational Global Forecast System based on FV3 (FV3GFS). This paper describes the
19 details of GEFS-Aerosols model development and evaluation of real-time and retrospective runs using different observations
20 from in situ measurement, satellite and aircraft data. GEFS-Aerosols predictions demonstrate substantial improvements for
21 both composition and variability of aerosol distributions over those from the former operational [NGACv2](#) system with the
22 fundamental updates ([e.g. dust and fire emission](#)) in atmospheric and chemical transport model.

Deleted: NGAC

Deleted: NGAC

1 **1. Introduction**

2 The operational air quality predictions in National Oceanic and Atmospheric Administration (NOAA)'s National Weather
3 Service (NWS) contribute to the protection of lives and health in the US (<https://airquality.weather.gov>). These predictions are
4 used by state and local air quality forecasters to issue official air quality forecasts for their respective areas. The U.S.
5 Environmental Protection Agency (EPA) and the Centers for Disease Control and Prevention (CDC) also use the NOAA
6 forecasts for applications with wildfire, health and smoke vulnerability assessments. Exposure to fine particulate matter, i.e.,
7 aerosol particles with diameters of 2.5 µm and smaller (PM_{2.5}), is recognized as a major health concern and the associated
8 mortality rate is estimated to be higher than the five specific causes of death examined by the global burden of disease [GBD,
9 Burnett et al., 2018].

10 ~~It is well known that the~~ role of aerosols in Numerical Weather Prediction (NWP), through interaction with atmospheric
11 radiation and precipitation physics (direct, semidirect, and indirect effect), and their impact on meteorological fields in both
12 weather and climate scale, have been widely recognized in many studies [e.g. Fast et al. 2006, Levin and Cotton, 2009; Chen et
13 al., 2011; Grell et al. 2011; Forkel et al. 2012; Muhlbauer et al., 2013; Xie et al., 2013; Yang et al., 2014; Wang H. et al., 2014,
14 Wang Q. et al., 2014]. ~~Additional studies at operational weather centers indicate the importance of including aerosol feedback~~
15 ~~in NWP for operational forecasting [Rodwell and Jung, 2008; Reale et al., 2011; Mulcahy et al., 2014; Bozzo et al. 2020]. At~~
16 National Centers for Environmental Prediction (NCEP), the operational RAPid refresh (RAP) and High-Resolution Rapid
17 Refresh (HRRR) storm scale modeling systems now include the impact of aerosols from biomass burning emissions on
18 radiation. Due to the importance of aerosol feedback in NWP, the performance of predicted aerosols and their optical properties
19 are critical before implementing the aerosol direct and semi-direct effect in NWP.

20 ~~Since last decade, global aerosol modeling grows rapidly to provide operational prediction and air quality alters in NWP. More~~
21 ~~than 15 years ago, NASA implemented an aerosol transport module, Goddard Chemistry Aerosol Radiation and Transport~~
22 ~~model (GOCART), online within the its Global Modeling and Assimilation Office (GMAO) Goddard Earth Observing System~~
23 ~~version 4 (GEOS-4) atmospheric general circulation model (AGCM) [Bloom et al., 2005], which is able to run in climate, data~~
24 ~~assimilation and replay modes [Colarco et al., 2010]. Later on, it switched to the next version of GEOS-5 to provide near-real~~
25 ~~time forecast of aerosols and atmospheric compositions [Rienecker et al., 2008; Molod et al., 2015]. Since 2008, as part of the~~
26 ~~project Global and regional Earth-system Monitoring using Satellite and in situ data (GEMS) the European Centre for Medium-~~
27 ~~Range Weather Forecasts (ECMWF) began to provide aerosol forecast [Hollingsworth et al., 2008; Morcrette et al., 2009;~~
28 ~~Benedetti et al. 2009]. In 2010, the International Cooperative for Aerosol Prediction (ICAP) was founded with one of its goals~~
29 ~~being the development of a global multi-model aerosol forecasting ensemble (ICAP-MME) for basic research and eventual~~
30 ~~operational use [Benedetti et al., 2011; Reid et al., 2011; Colarco et al., 2014]. In the ICAP, the complete aerosol forecast~~
31 ~~models are original from European Centre Medium Range Weather Forecasts Copernicus Atmosphere Monitoring Service~~
32 ~~(ECMWF-CAMS), the Japan Meteorological Agency Model of Aerosol species in the Global Atmosphere (JMA-~~

Deleted: The

Moved down [1]: et al., 2010].

Deleted: For example, global and regional models established a connection between dust emissions and weather patterns over synoptic-to-seasonal time scales [Haustein et al., 2012; Zhao

Deleted: Results from NASA's Goddard Earth Observing System (GEOS-5) forecasting system showed that the net impact of the interactive aerosol associated with a strong Saharan dust outbreak resulted in a temperature enhancement at the lofted dust level and a reduction near the surface levels, which improved forecasts of the African easterly jet (AEJ) [Reale et al., 2011]. Furthermore, the microphysical and thermodynamic effects from aerosols may play a role in impacting development of tropical cyclones [Rosenfeld et al. 2012].

Deleted: . The inclusion of the direct and indirect effects of aerosols in the global NWP configuration of the Met Office Unified Model (Met UM) indicated that using prognostic aerosols led to better temporal and spatial variations of atmospheric aerosol optical depth (AOD) and was of particular importance in cases of large sporadic aerosol events such as large dust storms or forest fires [Mulcahy et al., 2014]. At ECMWF, Rodwell and Jung [2008] showed an improvement in forecast skill and general circulation patterns in the tropics and extra-tropics by using a monthly aerosol climatology rather than a fixed climatology in the ECMWF global forecasting system. Later on, ECMWF replaced the aerosol climatologies with aerosols from a reanalysis of atmospheric composition produced by the Copernicus Atmosphere Monitoring Service [Bozzo et al, 2020].

Formatted: Pattern: Clear

Formatted: Pattern: Clear

Moved (insertion) [1]

1 [MASINGAR](#)), the National Aeronautics and Space Administration (NASA) Goddard Earth Observing System Version 5
2 (NASA-GEOS-5) and the Naval Research Lab Navy Aerosol Analysis and Prediction System (NRL-NAAPS) modeling
3 systems. There are also dust Dust-only model from the Barcelona Supercomputer Center Chemical Transport Model
4 (NMMB/BSC-CTM), the United Kingdom Met Office Unified Model (UKMO-UM) and National Oceanic and Atmospheric
5 Administration/National Centers for Environmental Prediction (NOAA NCEP) Environmental Modeling System (NEMS)
6 Global Forecast System (GFS) Aerosol Component (NGAC) [Sessions et al., 2015]. Xian et al. [2019] summarized and
7 compared the current states and performances of these global operational aerosol model in ICAP. The aerosol feedback is no
8 included into these operational models, and they are mostly driven by independent operational/quasi-operational
9 meteorological models developed at different NWP/research center with different vertical and horizontal resolution. All these
10 models include the major aerosol species of black carbon (BC), organic carbon (OC), sulfate, sea salt and dust. GEOS-5 has
11 extra trace of nitrate. The AOD root mean square error (RMSE) between ICAP-MME and 21 representative sites of AERONET
12 from 2012 to 2017 indicates improvements for find-mode AOD, while it shows small signals of potential model improvement
13 over the regions where is impacted by the biomass burning emission and dust [Xian et al., 2019].

14 NCEP, in collaboration with the NASA/Goddard Space Flight Center (GSFC), developed the NEMS Global Forecast System
15 (GFS) Aerosol Component version 1 (NGACv1) for predicting the distribution of global atmospheric aerosols [Lu et al., 2010].
16 NGAC is an interactive atmospheric aerosol forecast system with the NEMS global spectral model (NEMS GSM) as the
17 atmosphere model and GOCART as the aerosol model [Wang et al., 2018]. NGACv1 was implemented in 2012 and provided
18 the first operational global dust aerosol forecasting capability at NCEP [Lu et al., 2016]. In NGACv1 an in-line aerosol module
19 based on the Goddard Chemistry Aerosol Radiation and Transport (GOCART) model from GEOS-5 [Chin et al., 2000], but
20 limited to dust only, was used. The NGACv1 used the Earth System Modeling Framework (ESMF) to couple the aerosol
21 module with the GFS. Later, NCEP implemented a multispecies aerosol forecast capability NGACv2, based on NGACv1
22 through collaborations among NCEP, NASA/GSFC, the NESDIS Center for Satellite Applications and Research (STAR), and
23 the State University of New York at Albany [Wang et al., 2018].

24 In July 2016, NOAA took a significant step toward developing a state-of-the-art global weather forecasting model by
25 announcing the selection of a new dynamic core developed at NOAA Geophysical Fluid Dynamics Laboratory (GFDL) to
26 upgrade the GFS. The GFDL Finite-Volume Cubed-Sphere Dynamical Core (FV3) replaced the spectral GFS core in June of
27 2019 to drive global NWP systems with improved forecasts of severe weather, winter storms, and tropical cyclone intensity
28 and track. NOAA is now on the way to integrate various operational applications into the Unified Forecast System (UFS), a
29 comprehensive, community-based coupled Earth modeling system, designed as both a research tool and the basis for NOAA
30 operational forecasting applications.

31 Here we describe a new aerosol model component developed through collaborative efforts among the Global Systems
32 Laboratory (GSL), the Chemical Science Laboratory (CSL), and the Air Resources Laboratory (ARL), Environmental

Deleted: on

1 Modeling center (EMC) and STAR. This aerosol component was implemented operationally on September 2020 to provide
2 five-day global aerosol forecasts with ~ 25 km horizontal resolution and 64 vertical layers from the surface to 0.2 hPa as one
3 member of the Global Ensemble Forecast System of version 12 (GEFSv12): GEFS-Aerosols v1. The aerosol component is
4 designed as an independent model component for the NOAA Environmental Modeling System (NEMS) framework and
5 includes a coupling interface based on the National Unified Operational Prediction Capability (NUOPC) Layer for model
6 interoperability. All chemistry, aerosol, and emission modeling processes reside and run within this model component. There
7 is not aerosol feedback on the atmospheric model of GEFS, and the aerosols are not in any way interactive with the radiation
8 and clouds. GEFS-Aerosols shows a substantial improvement for both composition and variability of aerosol distributions
9 over those from the previous global aerosol prediction system NGACv2. The model predicted global aerosol products from
10 GEFS-Aerosols are also used for other applications, such as to provide lateral boundary conditions for NOAA's regional
11 National Air Quality Forecast Capability (NAQFC), satellite sea surface temperature (SST) physical retrievals, and the global
12 solar insolation estimation [Wang et al., 2018].

13 The current study presents the development of GEFS-Aerosols and evaluations of its performance in real time and retrospective
14 experiments. Section 2 describes the coupling components of the GEFS-Aerosols member, including the atmospheric
15 component of FV3GFS model, the aerosol component, and the observation, reanalysis, and model data used for evaluation
16 and comparison. The emission inventories of both anthropogenic emission and biomass burning emissions and other chemical
17 input data are presented in Section 3. Section 4 and Section 5 are the evaluations of Day-1 real-time forecast since July 2019
18 and the Day-1 retrospective forecast for the ATom-1 periods of 2016 summer, respectively. The conclusions and future plans
19 are summarized in Section 6.

20 2. Model and data

21 2.1 Descriptions of GEFS-Aerosols

22 2.1.1 FV3GFS and GEFS-Aerosols

23 The global Finite-Volume cubed-sphere dynamical core (FV3) developed by GFDL was chosen by NOAA as the non-
24 hydrostatic dynamical core to be the Next Generation Global Prediction System (NGGPS) of the National Weather Service in
25 the US [Black et al., 2021]. Currently, the FV3 was successfully implemented within the physical scheme of GFS version 15
26 (named as FV3GFS v15), which became operational on June 2019. It has the capability to provide the metrological basis for
27 coupling with aerosol prediction component. The GEFS is a weather forecast modeling system made up of 31 separate forecasts,
28 or ensemble members, which have the same horizontal (~25 km) and vertical resolution (64 layers from the surface to 0.2 hPa).
29 The GEFS-Aerosols model is only using one of the same weather model as other GEFS members except it includes the
30 prognostic aerosols from the coupling aerosol component. The NCEP started the GEFS to address the nature of uncertainty

Deleted: NGAC

Deleted: , and the FV3-based GFS

Deleted: GFSv15)

Deleted: , providing

Deleted: a simple

Deleted: but

Deleted: . It is about 2.5 times computational cost when include...

Deleted: in the forecast. In the operation, there is no execution time since the it only performs 120 hours forecast with aerosol component, while other members without aerosol component would perform 384 hours forecast.

1 in weather observations that are used to initialize weather forecast models and uncertainties in model representation of
2 atmospheric dynamics and physics. The aerosol component coupled with FV3GFS v15 has been merged into the GEFS, as a
3 single ensemble member named as GEFS-Aerosols, for real-time and retrospective forecast that preceded operational
4 implementation, which occurred in September 2020.

5 In GFS v15, all sub-grid scale transport and convective deposition related to aerosol is handled inside the atmospheric physics
6 routines of simplified Arakawa-Schubert (SAS) scheme. It requires consistent implementation of positive definite tracer
7 transport and wet scavenging in the physics parameterizations, which was implemented subsequent in the forecast system of
8 GEFSv12.

- Deleted: All
- Deleted: , which required
- Deleted: GFSv15 and

9 2.1.2 Aerosol component

10 The current aerosol component in the GEFS-Aerosols model is based on the simple bulk aerosol modules from WRF-Chem
11 [Grell et al., 2005; Powers et al., 2017], and the first time to be used in the global model is the Flow-following finite-volume
12 Icosahedral Model (FIM), as FIM-Chem [Zhang et al, 2022], including aerosol modules from GOCART. The metrological
13 fields (such as land use and other climatological surface fields, vegetation type etc.) are imported from the FV3 atmospheric
14 model to the chemical model to drive the aerosols components. They are consistent in the FV3 atmospheric model and chemical
15 model. Other than the aerosols convective wet scavenging, all the chemical related processes of source and sink, such as
16 emission, dry deposition, settling, large-scale wet deposition, chemical reactions are handled by the chemical model. The large-
17 scale wet deposition and dry deposition modules are from WRF-Chem for GOCART aerosols scheme, which are column
18 model driven by meteorological input from atmospheric model. Large-scale wet removal of aerosols includes below-cloud
19 removal (washout) following Easter et al. [2004] and the details of below-cloud wet scavenging via interception and impaction
20 can be found in Slinn [1984]. The dry deposition is the same as Chin et al. [2002]. After updating the chemical tracers in
21 chemical model, they are passed back to FV3 atmospheric model for transport and advection.

22 The GOCART aerosol modules use simplified sulfur chemistry for sulfate simulation, bulk aerosols of BC, OC, and sectional
23 dust and sea salt [Chin et al., 2000]. For OC and BC, the hydrophilic and hydrophobic components are considered and the
24 chemical reactions for gaseous sulfur oxidations are calculated using prescribed OH, H₂O₂, and NO₃ fields for gaseous sulfur
25 oxidations [Chin et al., 2000]. The GOCART model background fields of prescribed OH, H₂O₂, and NO₃ have been replaced
26 by the newer version of 2015 from the NASA GEOS Global Modeling Initiative (GMI) Chemical transport model (<https://acd-ext.gsfc.nasa.gov/Projects/GEOSCCM/MERRA2GMI/>). These are monthly mean data and these prescribed OH, H₂O₂, and
28 NO₃ fields would not be transported and changed in space. The marine dimethyl sulfide (DMS) emission is calculated as a
29 product of sea water DMS concentration and sea-to-air transfer velocity as described by Chin et al., [2000]. Recently, some
30 modifications and updates have been implemented, including the biomass burning plume rise module adapted from High-
31 Resolution Rapid Refresh (HRRR)-Smoke based on WRF-Chem, the capabilities of using the version 3 biomass-burning

- Deleted: black carbon (
- Deleted:), organic carbon (
- Deleted:),

1 emission calculations based on the Blended Global Biomass Burning Emissions Product (GBBEPx, Zhang et al., 2014) and
2 Fire Radiative Power (FRP) data provided by NESDIS (GBBEPx v3) as well as the application of the global anthropogenic
3 emission inventories from Community Emissions Data System (CEDS).

4 The sea salt scheme was updated to the most recent version with five size bins based on NASA's 2nd-generation GOCART
5 model (Colarco et al., 2010). The model has the capability of handling volcanic eruptions, which need the estimate of injection
6 height and SO₂ and volcanic ash emissions. While for the predicted results in the paper, the volcanic emission has not been
7 included.

8 A new dust emission scheme, referred to as FENGSHA, was implemented in GEFS-Aerosols. The scheme, which is also used
9 in NOAA's National Air Quality Forecast Capability, is modified from the original Owen equation [Tong et al., 2017, Owen,
10 1964; Shao et al., 1993],

$$F = \sum_{j=1}^N K \times A \times \frac{\rho}{g} \times S \times u_* \times (u_*^2 - u_{*tj}^2) \quad \text{for } u_* > u_{*tj} \quad (1)$$

12 where N is the number of soil types in a particular grid cell, K is the ratio of vertical to horizontal emission flux, A represents
13 particle supply limitation (availability), ρ is air density, g is gravitational acceleration, S is the soil erodibility potential, u_* is
14 friction velocity, and u_{*tj} is the threshold friction velocity for soil type j [Shao et al., 1993]. Dust emission is calculated only
15 when friction velocity exceeds the designated threshold value for the land use type and soil texture. The threshold friction
16 velocities are based on wind tunnel measurements done in both the laboratory and field [Gillette et al., 1980].

17 What makes FENGSHA unique is the way in which the threshold values are determined. Unlike models based on Marticorena
18 and Bergametti [1995] or Shao et al., [2011], threshold values are based on surface and wind tunnel flux measurements of
19 saltation [Gillette, 1988]. The drag partition in the FENSGHA scheme is described by the MacKinnon et al. [2004]
20 parametrization using the model surface roughness (z_0) or derived from the surface roughness estimates using the Advanced
21 Scatterometer (ASCAT) as described by Prigent et al. [2012]. The Fécan et al [1998] soil moisture correction is used to adjust
22 the dry threshold friction velocity. Once the total windblown dust emission flux is computed the total flux is distributed into
23 the modeled dust bins using the Kok [2011] distribution.

24 A new sediment supply map, the Baker-Schepanski Map (BSM), which was developed from the ideas of Chappell and Webb
25 [2016] is currently used within the GEFS-Aerosol FENGSHA implementation. Chappell and Webb [2016] created an approach
26 similar to that of the Raupach [1992] model for lateral cover but instead uses a top-down view to describe the area of the
27 turbulent wake using an analogous shadow instead of a two-dimensional view. The shadow approach is sensitive to the
28 configuration of the roughness elements meaning that it is sensitive to the placement of the roughness elements in relation to
29 each other. The BSM describes the probability of momentum mixing directly to the soil surface through the canopy. For the
30 application into GEFS-Aerosols a monthly 3-year climatology of the BSM was created which refers to a monthly average over
31 3 observation years, in this case 2016, 2017 and 2018 as these were the latest full years at the time of model development.

Deleted: version 3

Deleted: v3] [

Deleted: emission

Deleted: capable

2.1.3 GEFS-Aerosols coupled architecture, running sequence and forecasting workflow

The aerosol component of GEFS-Aerosols couples directly to the FV3-based atmospheric component via the NUOPC Layer [Theurich et al., 2016], which is the foundation of NOAA's modeling framework (Fig. 1). Fig. 2a shows the model coupled structure that the aerosol component imports meteorological fields from the atmospheric model and exchanges aerosol mixing ratios at each coupling time step via standard NUOPC connectors. Each aerosol species is simulated as a prognostic atmospheric tracer, which is advected by the FV3 dynamical core and undergoes convective mixing and PBL diffusion within the atmospheric physics. All aerosol composition and emission-related processes are computed in GEFS-Aerosols after the atmospheric physics has been advanced and passed to the chemical model following the sequences as emission, settling of dust and sea salt, plume-rise of fire emission, dry deposition, large-scale wet deposition, chemical reactions and carbonaceous aerosol updating. Tracer mixing ratios are then updated and exported back to the atmospheric model.

Bundling all aerosol composition processes in a single model component led to the implementation of a sequential coupling scheme with the atmospheric component. At each coupling time step, the atmospheric dynamical core and physics processes (including radiation) are computed first. The aerosol component is then executed to perform all air composition processes and transfer the updated tracers back to the atmospheric component. Finally control returns to the atmospheric model, which updates the atmospheric state with new meteorology and aerosols concentrations. To minimize overhead associated with data exchange between model components, GEFS-Aerosols is run on the atmospheric grid, which is imported from the atmospheric component through NUOPC. Additionally, the coupling run sequence assigns to the aerosol component the identical set of Persistent Execution Threads (PETs) used by the atmospheric model's forecast component. This allows the model to leverage NUOPC's ability to access coupling fields by memory reference, minimizing the memory footprint for the coupled system.

The sequence of steps involved in moving from the beginning to the end of a forecast process is controlled by the workflow. In a retrospective or real time forecast, the chemical tracers are cycled from the output of a previous forecast as the initial condition. In operation, the computational cost with aerosol component would take 129 mins for 120 hours forecast. Therefore, the efficiency is about 2.53 times computational cost by including aerosol component compared to the one without aerosol component in the forecast. In the operation, there is no execution time by including the aerosols component as one of the ensemble members since this member only performs 120 hours forecast by including aerosol component, which is shorter than other members without aerosol component that perform 384 hours forecast.

The workflow shown in Figure 2(b) describes the steps including pre-processing (prepare input data) and post-processing (process output data) before and after forecast for the GEFS-Aerosols in the forecast system. This initial implementation of GEFS-Aerosols does not include aerosol data assimilation, so the chemical tracers in the restart files are used as the chemical initial condition for the next forecast. The yellow box includes the tasks/steps for atmospheric mode, while the green box includes the tasks/steps for chemical model. The AOD is calculated in the post-processing part of the workflow, using a look-

1 up table (LUT) of aerosol optical properties from NASA GOCART model [Colarco et al. 2010, Colarco et al. 2014], which
2 was implemented in the Unified Post Processor (UPP, <https://dtcenter.org/community-code/unified-post-processor-upp>). It
3 should be noted that the LUT reflects the impacts of a larger number of aerosol species in the atmosphere than the simple
4 GOCART module treats. Also, considering the bulk aerosol scheme in GOCART, there is no size distribution for OC, BC and
5 sulfate, the LUT may have uncertainties in the AOD calculation. Based on observational validation, some adjustments have
6 been applied in into LUT calculation to compensate the contributions for the absence of nitrate, ammonium and secondary
7 organic aerosol (SOA) in GOCART.

Deleted: with factor of 2

8 2.2 Observation, reanalysis data and other model data

9 The real-time forecast experiments were evaluated using the following ensemble analysis, reanalysis data, satellite and in situ
10 observational data, aircraft measurements, and model predictions. We compare each day model forecast hours with same day
11 reanalysis or analysis data and compute the AOD statistics (e.g. bias, RMSE, correlation etc.) for each grid for each pair of
12 model and reanalysis or analysis data for that model forecast hour. We then calculate that for the entire 4 months of the study
13 period and averaged it over the entire 4 months for each grid points. This method gives an overall estimate of systematic bias
14 of the model in spatial and temporal scale.

15 2.2.1 Reanalysis data of AOD

- 16 1) Total AOD instantaneous reanalysis dataset from the second Modern-Era Retrospective analysis for Research and
17 Application [MERRA-2, Gelaro et al., 2017]. The MERRA-2 reanalysis provides various AOD product at 0.625 x
18 0.5 degree horizontal resolution and at 72 vertical levels. MERRA-2 reanalysis data is not synchronous as real-time,
19 and normally has 1-2 months' time lag.

20 2.2.2 Observation data of Satellite AOD, AERONET AOD and ATOM-1 concentration.

- 21 1) MODIS provides near-global coverage of aerosol measurements in space and time. We have used a MODIS Level-3
22 (daily and monthly at 1 degree horizontal resolution) AOD dataset in this study (<https://ladsweb.nascom.nasa.gov/>).
23 The dataset belongs to the Collection 6.1 combined land and ocean from the Aqua satellite [Levy et al., 2013]. This
24 latest collection of MODIS data includes AOT data based on refined retrieval algorithms, in particular the expanded
25 Deep Blue algorithm [Hsu et al., 2013; Sayer et al., 2013]. It introduces a merged AOD product, combining retrievals
26 from the Dark Target (DT) and Deep Blue (DB) algorithms to produce a consistent data set covering a multitude of
27 surface types ranging from oceans to bright deserts [Sayer et al., 2014]. In this work the aerosol product
28 Dark_Target_Deep_Blue_Combined_Mean was used for quantitative evaluation of model results. We have used
29 Collection 6.1 MODIS AOD at 550nm, which has Expected Errors (EEs) of [$\pm (0.05 + 15\%AOD)$] and [$\pm (0.03 +$
30 $5\%AOD)$] for Dark Target retrievals at a 10-km resolution over land and ocean, respectively. The EEs are

1 approximately [$\pm (0.03+21\%AOD)$] for 'arid' and [$\pm (0.03+18\%AOD)$] for 'vegetated' path Deep Blue retrievals at
2 a 10-km resolution over land [Levy et al., 2013].

3 2) The Visible Infrared Imaging Radiometer Suite (VIIRS) sensor onboard the Suomi National Polar Orbiting (S-NPP)
4 satellite provides sets of aerosol environmental data records (EDRs) based on daily global observations from space
5 [Jackson et al., 2013; Liu et al., 2013]. Beginning in 2012, VIIRS provides AOT at 550 nm at a global 0.25 degree
6 horizontal resolution. Daily gridded Enterprise Processing System (EPS) VIIRS data used are from the NOAA STAR
7 ftp site at ftp://ftp.star.nesdis.noaa.gov/pub/smcd/VIIRS_Aerosol/npp.viirs.aerosol.data/epsaot550/.

8 3) The Aerosol Robotic Network (AERONET), which is a global ground-based network of automated sun-photometer
9 measurements, provides AOT, surface solar flux and other radiometric products [Holben et al., 1998]. It is a well-
10 established network of over 700 stations globally and its data are widely used for aerosol-related studies [Zhao et al.,
11 2002]. AERONET employs the CIMEL sun-sky spectral radiometer, which measures direct sun radiances at eight
12 spectral channels centered at 340, 380, 440, 500, 675, 870, 940 and 1020 nm. AOT uncertainties in the direct sun
13 measurements are within ± 0.01 for longer wavelengths (longer than 440 nm) and ± 0.02 for shorter wavelengths [Eck
14 et al., 1999]. Table 1 lists number of stations, their location in terms of latitude and longitude. The stations are selected
15 based on years in service and geographic location near the aerosol source regions. Stations covered major aerosol
16 sources: African Dust, Southern Africa and South America (major forest fire stations), mixed aerosol regimes (urban
17 areas in Europe, Asia and N. America), high latitude stations (capture major transport of forest fires from Siberia and
18 Canada).

19 4) The Atmospheric Tomography Mission (ATom) studies the impact of human-produced air pollution on greenhouse
20 gases and on chemically reactive gases in the atmosphere [Wofsy et al., 2018]. ATom deploys instrumentation to
21 sample atmospheric composition, profiling the atmosphere in 0.2 to 12 km altitude range. Flights took place in each
22 of 4 seasons over a 22-month period in 2016 through 2018. They originated from the Armstrong Flight Research
23 Center in Palmdale, California, flew north to the western Arctic, south to the South Pacific, east to the Atlantic, north
24 to Greenland, and returned to California across central North America over the Pacific and Atlantic oceans from ~
25 80°N to ~ 65°S. In August 2016, PALMS was sampling on the NASA DC-8 aircraft as part of the ATom program
26 (<https://espo.nasa.gov/missions/atom/content/ATom>). Aerosol composition determinations using the PALMS
27 instrument during ATom-1 have been described and interpreted previously [Murphy et al., 2018, 2019; Schill et al.,
28 2020; Bourgeois et al., 2020]. The PALMS mass concentrations for various species are derived by normalizing the
29 fractions of particles of each size and type to size distributions measured by optical particle counters [Froyd et al.,
30 2019].

31 2.2.3 Model ensemble analysis AOD and other model forecasts

1) International Centers for Aerosol Prediction - Multi-Model Ensemble (ICAP-MME) provides daily 6-hourly forecasts of total and dust AOD globally out to 120 h at 1 degree horizontal resolution [Reid et al., 2011; Sessions et al., 2015; Xian et al., 2019]. Total AOD in ICAP-MME is provided by the four core multispecies models: the European Centre Medium Range Weather Forecasts Copernicus Atmosphere Monitoring Service (ECMWF-CAMS), the Japan Meteorological Agency Model of Aerosol species in the Global Atmosphere (JMA-MASINGAR), the NASA Goddard Earth Observing System Version 5 (NASA-GEOS-5) and the Naval Research Lab Navy Aerosol Analysis and Prediction System (NRL-NAAPS) modeling systems. Dust-only AOD is provided by the aforementioned four models, plus the Barcelona Supercomputer Center Chemical Transport Model (NMMB/BSC-CTM), the United Kingdom Met Office Unified Model (UKMO-UM) and NGACv2. However, the NGACv2 is only used for dust AOD in ICAP-MME, not use to compute ensemble mean in ICAP-MME for total AOD. All four of the multispecies models incorporate aerosol data assimilation (DA) and satellite-based smoke emissions. ICAP-MME is able to provide real-time comparison for synchronous evaluation of operational forecast. The correlation and RMSE between ICAP-MME and AERONET indicating in Table 1 shows that ICAP analysis is quite close to observation, which is good to use it as the global evaluated data, especially when the MERRA-2 data is not available in the real-time or operational forecast.

2) The NEMS GFS Aerosol Component Version 2.0 (NGACv2) for global multispecies aerosol forecast developed by NCEP and collaborators was previously used to provide operational global multispecies aerosol forecasts at NCEP [Wang et al., 2018]. The anthropogenic emissions are based on EDGAR V4.1 [Janssens-Maenhout, 2010] and AeroCom Phase II [Diehl et al., 2012]. The ~~fire Emissions of carbonaceous aerosols and SO2 are from Global Biomass Burning Emission Product-extended [GBBEPx, Zhang et al. 2014]. GBBEPx emissions are blended from NESDIS's Global Biomass Burning Emission Product from a constellation of geostationary satellites [GBBEP; Zhang et al., 2012] and GMAO's Quick Fire Emissions Data Version 2 from polar-orbiting satellites [QFED2; Darmenov and da Silva, 2015].~~

3) NGACv2 uses the same physics package as the 2015 version of the operational GFS. NGACv2 included additional aerosol species of sea salt, sulfate, organic carbon, and black carbon from the updated GOCART modules. Both science and software upgrades in the global forecast system were updated and implemented into NGACv2 in March 2017 to provide 5-day multispecies aerosols forecast products at the T126 L64 resolution, approximately 100 km. The comparison of model configurations for GEFS-Aerosols and NGACv2 has been shown in Table 2 based on the model information from Wang et al. [2018].

- Deleted: smoke
- Deleted: from NESDIS STAR's GBBEPx,
- Deleted: the global biomass burning emission product
- Deleted: -Geo, Zhang et al., 2012
- Deleted: 2014
- Deleted: GSFC's
- Deleted: Emission
- Deleted: a
- Deleted: sensor
- Deleted: ,
- Deleted:
- Deleted:

3. Emissions

3.1. Anthropogenic emissions and background fields

1 The preprocessor PREP-CHEM-SRC v1.7, a comprehensive tool that prepares emission fields of trace gases and aerosols for
2 use in atmospheric chemistry transport models, was used to generate the anthropogenic emissions, background fields of OH,
3 H₂O₂, NO₃, DMS and dust scheme input of clay and sand at the FV3 grid resolution for GEFS-Aerosols [Freitas et al., 2011].
4 Two global anthropogenic emission inventories were chosen as input to drive the model, both providing monthly emissions.
5 One is from the Community Emissions Data System (CEDS), which provides the emissions of BC, OC and SO₂ in 2014 with
6 0.5 degree horizontal resolution [Hoesly et al., 2018]. The CEDS inventory improves upon existing inventories with a more
7 consistent and reproducible methodology applied to all emission species, updated emission factors, and more recent estimates
8 in 2014. The data system relies on existing energy consumption data sets and regional and country-specific inventories to
9 produce trends over recent decades [Hoesly et al., 2018]. The Hemispheric Transport of Air Pollution (HTAP) version 2
10 [Janssens-Maenhout et al., 2015] inventory provides the emissions of BC, OC SO₂, PM_{2.5} and PM₁₀ in 2010.
11 Figure 3 shows the comparisons of anthropogenic emissions between CEDS and HTAP for SO₂, BC and OC in July. Aside
12 from the shipping lanes showing up in CEDS, there is generally broader spatial coverage in CEDS. For SO₂, the CEDS
13 emissions are much larger over the eastern US, eastern China and Europe. Much higher values of BC and OC are seen in
14 CEDS over Eastern Asia, South Asia and Europe. Similarly, much larger values for BC and OC are seen in the Southern
15 Hemisphere in CEDS. We performed experiments by comparing model predictions using these two different anthropogenic
16 emissions datasets with ATom-1 observations (figures not shown here). Slight improvements in SO₂ correlations and bias are
17 seen and the sulfate, OC and BC biases improve over the Atlantic Ocean when using the CEDS emissions in comparison with
18 the HTAP dataset. It should be noted that these anthropogenic emissions data are not impossible to catch up the date of real-
19 time forecast. And it normally has time lag and represents the emissions of a different previous years. The inconsistency may
20 have some impact on the predictions in 2019. But that is the most recently available version of anthropogenic emission. It is
21 well known that strong actions have been taken to improve the worsening atmospheric environment and decrease the emission
22 over China in the last 10 years [Chen et al., 2017; Zhang et al., 2012; Liu et al., 2016]. Considering the decreasing emission
23 trend over China, the CEDS 2014 anthropogenic would result in some overprediction after 2014.
24 We validated the GOCART background fields of OH and H₂O₂ against the ATom-1 observations. Even though these
25 background fields are model-derived climatologies, they both compare very well with the ATom-1 measurements. The newer
26 NASA GEOS/GMI fields show improvement in the model-measurement biases for both OH and H₂O₂.

27 3.2 Biomass burning emission

28 The operation of GEFS-Aerosols is using the GBBEPx v3 emission with Fire Radiative Power (FRP). The GBBEPx v3 system
29 produces daily global biomass burning emissions of PM_{2.5}, BC, CO, CO₂, OC, and SO₂) by blending fire observations from
30 MODIS Quick Fire Emission Dataset (QFED), VIIRS (NPP and JPSS-1) fire emissions, and Global Biomass Burning
31 Emission Product from Geostationary satellites (GBBEP-Geo). GBBEP-Geo also produces hourly emissions from

1 geostationary satellites, at individual fire pixels. In the results shown here, GBBEPx v3 daily biomass burning emissions on
2 the FV3 C384 global grid are used for GEFS-Aerosols. The details of the GBBEPx v3 algorithm can be found in
3 https://www.ospo.noaa.gov/Products/land/gbbepx/docs/GBBEPx_ATBD.pdf.

4 A one-dimension (1-D) time-dependent cloud module from High-Resolution Rapid Refresh (HRRR)-Smoke model has been
5 implemented into GEFS-Aerosols to calculate injection heights and emission rates online [Freitas et al., 2007]. The new
6 scheme in HRRR-Smoke is a modified version of the 1D plume rise scheme used in WRF-Chem [Freitas et al., 2007]. The
7 new plume rise scheme is using the FRP data instead of the look-up table to estimate the fire heat fluxes [Ahmadov et al,
8 2017]. The 1-D cloud module is able to be applied ~~GBBEPx v3 fire emissions datasets to account for plume-rise that distributes~~
9 the fire emissions vertically and better simulate the fire events and pollution transport of smoke plumes.

10 To validate model performance when using the GBBEPx v3 fire emissions with a plume-rise module based on real-time FRP
11 data, we compare the real-time GEFS-Aerosols AOD with other reanalysis data, satellite observations and the NGACv2 model
12 for the big fire event in August 2019. Smoke from large fires burning in the Amazon rainforest, primarily in Brazil, Bolivia,
13 Paraguay, and Peru, stretched over northern South America in mid-August. Figure 4 shows the total AOD forecast on 25th
14 August compared against the NGACv2 model, MERRA-2 reanalysis data and satellite observations of VIIRS and MODIS.
15 For both satellites, daily gridded AOD is used to compare against the model forecast at 18z. The GEFS-Aerosols AOD is able
16 to reproduce the enhanced AOD due to several fire events over South America near the border of Bolivia, Paraguay, and Brazil,
17 which were also observed by the VIIRS and MODIS satellite instruments and captured by the MERRA2 analysis. Although
18 there are a lot of missing data downwind from the fires in the satellite observations of VIIRS and MODIS, especially over the
19 south Pacific, GEFS-Aerosols and MERRA-2 results are consistent in showing the transport of fire plumes into the tropical
20 Pacific and southern Atlantic. In contrast, the NGACv2 model does not capture these fire events, and exhibits only a very
21 slight AOD enhancement. NGACv2 AOD is more than 80% smaller than the observations over the fire source region and
22 produces little or no transported smoke over the surrounding areas.

23 Beyond the fires burning in South America, an even greater number of blazes on the African continent are observed by the
24 satellite images at almost the same time in August 2019. Angola experienced almost three times more fires than Brazil in the
25 middle of August 2019. There were around 6,000 fires in Angola, more than 3,000 in Congo and just over 2,000 in Brazil,
26 according to NASA satellite imagery (<https://earthobservatory.nasa.gov/images/145421/building-a-long-term-record-of-fire>).

27 One of the main large-scale aerosol features of Sub-Saharan Africa is the June-to-September biomass burning season in Angola,
28 Congo, and Zambia [Bauer et al., 2019]. Overall, the GEFS-Aerosols model reasonably simulates the major burning event on
29 August 25th, 2019 over southern Africa (Figure 4), but overestimates the central African plume when compared with the
30 MERRA2 analysis. The satellite AOD retrievals of VIIRS and MODIS off the coast of central Africa are challenging due to
31 screening by the stable stratiform cloud deck over the ocean that occurs during the fire season, creating less reliable coverage
32 from these observational data. Nevertheless, we can still see consistent AOD enhancements over the fire source regions and

Deleted: https://www.ospo.noaa.gov/Products/land/gbbepx/docs/GBBEPx_ATBD.pdf

Deleted: with these two different

1 surrounding areas for both GEFS-Aerosols and the observations. NGACv2, however, is quite different from the satellite
2 observations and MERRA2 analysis, underestimating the AOD more than 50-90% percent over the southern Africa fire source
3 region and showing little obvious enhancement. [Obviously, the updates in fire emission using GBBEPx v3 emission and FRP
4 by applying the 1D plume rise scheme in GEFS-Aerosols model show great improvements in the AOD forecast during the fire
5 events compared to the NGACv2 \(Table 2\).](#)

6 Future work will explore the use of diurnal fire profiles based on historic GOES fires products applied to estimate biomass
7 burning emissions to enhance forecast behavior. Additionally, a parameterization based on fire weather index (FWI) to
8 estimate biomass burning emissions on longer temporal scales may help to improve and extend the forecast of fire impacts.

9 4. Real-time forecast Evaluation

10 4.1 Evaluation of global AOD

11 A real-time forecast was performed starting on July 1 2019 on ~25km resolution and continuing to the present day using the
12 GBBEPx v3 fire emissions with the plume-rise module based on real-time FRP data.

13 We evaluated the GEFS-Aerosols model performance with the daily AERONET data globally. The locations of the 60 selected
14 AERONET sites where these comparisons were made are listed in Table 1. It also indicates the correlation and RMSE of
15 GEFS-Aerosols, ICAP and NGACv2 AOD with respect to that of AERONET observation. The GEFS-Aerosols, NGACv2
16 and ICAP predictions are sampled at the same locations as the AERONET sites for these comparisons. The left panel in Figure
17 5 (a and b) shows the correlation coefficients between daily total AOD observed by AERONET and the day 1 forecast of
18 model AOD from GEFS-Aerosols and NGACv2 for the period between 7/5/2019 and 11/30/19. The correlation coefficients
19 range from 0.5 to 0.9 for GEFS-Aerosols at most sites, except for several sites in South America, Africa and eastern Asia near
20 fire source regions, which are slightly lower than those of the ICAP. In contrast, the correlation coefficients of daily total AOD
21 between the NGACv2 and AERONET observations are lower than 0.5 globally, even ranging from 0.1 to 0.3 at most sites. A
22 more quantitative display of correlation coefficients for a selection of 60 AERONET sites for GEFS-Aerosols and NGACv2
23 is presented in Table 1. This comparison strongly indicates the improved performance of total AOD daily variation in GEFS-
24 Aerosols prediction when compared with NGACv2. There are 20 sites (about 30% of total sites) displaying highly correlated
25 total AOD for the AERONET data and GEFS-Aerosols, with the correlation coefficients exceeding 0.7. In contrast, there is
26 only 1 site with a correlation coefficient larger than 0.7 for NGACv2 model vs. AERONET, and 19 sites have correlation
27 coefficients that are less than 0.2 for AERONET and NGACv2. Fig. 5 c and are the RMSE of GEFS-Aerosols and NGACv2
28 with respect to AERONET observation. Most of RMSE values are below 0.25 in GEFS-Aerosols over North America, Europe
29 and Africa. However, the RMSE values in a lot of sites over Africa and Asia are above 0.3 in NGACv2. From Table 1, the
30 ICAP results show the best performance in both the correlation and RMSE.

Deleted: root mean square error (

Deleted:)

1 In addition to comparing with the AERONET data, Fig. 6 shows the Day 1 AOD prediction of GEFS-Aerosols and NGACv2
2 compared with the MERRA-2 reanalysis and MODIS observations averaged from July to November 2019. The GEFS-
3 Aerosols prediction is able to capture the geographical features of AOD as represented by the MERRA-2 reanalysis data and
4 MODIS satellite observations, such as the dust plumes over North Africa and the Arabian Peninsula, biomass burning plumes
5 in southern Africa, south America, northwestern America and eastern Europe, polluted air over eastern and southern Asia, and
6 high-latitude sea-salt bands over the southern hemisphere. The high AOD over southern Africa and northern India is more
7 comparable to the MODIS observation, that of NGACv2. As pointed out by Bhattacharjee et al. [2018], the NGACv2
8 predictions exhibit widespread underestimates over most of these high AOD regions, such as eastern Asia, and fire source
9 regions of southern Africa, eastern Europe, southeastern Asia.

10 Figure 7 indicates the Day 1 AOD forecast biases of GEFS-Aerosols and NGACv2 with respect to MERRA-2 reanalysis
11 between 7/5/2019 and 11/30/19 for dust, OC and sulfate. The predicted dust AOD in GEFS-Aerosols is quite comparable to
12 that of MERRA-2 results, with only small negative biases of ~ 0.08 over Asia and the downwind areas of African dust source
13 regions of Atlantic and south Asia (Figure 8a). GEFS-Aerosols has some small positive biases relative to MERRA-2 of ~ 0.1
14 over Australia (in red). In contrast, dust AOD in NGACv2 (Figure 8b) shows large over predictions of MERRA-2 over Africa
15 with maximum value ~ 0.45 and about $0.02-0.05$ over large areas of Asia and North Pacific and North America. Wang et al.
16 [2018] also showed that the predicted dust AOD in NGACv2 over northwestern Africa is much larger than GEFS-Aerosols,
17 MERRA-2 and MODIS observations.

18 OC is a major component emitted from wildfires, and OC AOD is a good indicator of the performance of fire impacts. GEFS-
19 Aerosols OC AOD shows smaller biases compared to the MERRA-2 reanalysis than those of NGACv2 (Figure 7c and d).
20 Positive biases in GEFS-Aerosols OC AOD of less than 0.2 occur mainly over southern Africa, eastern Asia, south Asia and
21 the Middle East. The GEFS-Aerosols overprediction of OC AOD compared with MERRA-2 over eastern China may be
22 associated with the overestimate of anthropogenic emissions by using CEDS 2014, since this is not a major fire source region.
23 GEFS-Aerosols shows small negative biases, of less than 0.1, over South America and middle and eastern Europe. Overall,
24 the biases of OC AOD in NGACv2 relative to MERRA-2 are dominated by under prediction globally with the largest biases
25 of more than 0.3 over major fire source regions of southern Africa, the Amazon region of South America, Southeastern Asia
26 and Siberia (Figure 7d).

27 For sulfate AOD, the GEFS-Aerosols forecast over predicts MERRA-2 by ~ 0.08 over eastern Africa, the Middle East, and
28 southeastern China, where SO_2 anthropogenic emissions are dominant. Small GEFS-Aerosols under predictions, less than 0.1
29 AOD, are seen over broad areas of the Northern Hemisphere, such as eastern North America and its downwind areas over the
30 north Atlantic and western Europe, as well as eastern Asia and its downwind areas (Figure 7e). As in the case of OC AOD,
31 the global sulfate AOD in MERRA-2 is under predicted significantly by NGACv2 (Figure 7f). The areas with the largest

Deleted: .

1 NGACv2 vs. MERRA-2 sulfate bias are mainly over the major anthropogenic source regions, such as India and eastern China,
2 where the underestimates exceed 0.18, and in the eastern US and western Europe, where they exceed 0.1.
3 The summary comparison of the GEFS-Aerosols and NGACv2 Day 1 total AOD prediction biases with respect to MERRA-2
4 reanalysis between 7/5/19 and 11/30/19 is shown in Figure 8. Generally, the GEFS-Aerosols model is able to reproduce the
5 total AOD very well, much better than NGACv2 (see Figure 8a and b). The GEFS-Aerosols over predictions over eastern
6 China and Southern Hemisphere ($\sim 0.2-0.3$) are mainly due to anthropogenic OC and SO₂ for the former and fire emissions of
7 OC for the latter, respectively. Both GEFS-Aerosols and NGACv2 total AOD have small negative biases ($\sim 0.3-0.5$) relative
8 to MERRA-2 over the northwestern China dust source region. Negative biases of GEFS-Aerosols vs. MERRA-2 in South
9 America may be caused by inadequate fire emissions and in Europe that may be related to anthropogenic SO₂ emissions. The
10 spatial locations of biases in GEFS-Aerosols with respect to MERRA-2 reanalysis total AOD (Figure 8a) are similar to the
11 comparisons with the individual aerosol species from MERRA-2 discussed above (Figure 7a, c and e). The NGACv2 total
12 AOD is biased low relative to MERRA-2 almost globally except for the over prediction over North Africa due to dust (Figure
13 8b). The largest NGACv2 total AOD biases are mainly caused by the under predictions of fires over the fire source regions of
14 South America, southern Africa, Southeastern Asia and middle and eastern Europe and the anthropogenic source regions over
15 eastern China, India and eastern North America, with maximum total AOD biases reaching more than 0.5.

16 4.2 Evaluation of AOD associated with fire events

17 We choose some sites near the major fire source region, which have available observation data for the duration of this study
18 and hold long records based on various previous studies. Figure 9 indicates the total AOD time series of AERONET
19 observations compared against ICAP, NGACv2 and GEFS-Aerosols model predictions at the four AERONET sites near the
20 fire source regions of South America during the period of 7/1/19-11/30/19. At the Alta Floresta site, which is in the middle of
21 Amazon fire source region, the daily AOD variations of both the ICAP and GEFS-Aerosols day 1 predictions are quite
22 consistent with that of the AERONET data, especially as they are able to reproduce two peaks in AOD enhancements in late
23 August and late September caused by fire plumes (Figure 9a). The correlation (RMSE) is 0.66 (0.23), 0.9 (0.12) and 0.68 (0.31)
24 for GEFS-Aerosols, ICAP and NGACv2. Obviously, NGACv2 results under predict AERONET observations almost
25 throughout the whole period with a significantly larger bias than GEFS-Aerosols or ICAP, and the two August-September
26 peaks in total AOD enhancements are essentially missed in the NGACv2 prediction.

27 The Itajuba site is located southeast of the Alta Floresta site and in the downwind areas of the Amazon fire source region. The
28 total AOD time series of GEFS-Aerosols prediction matches closely those of ICAP and AERONET during most of the time
29 period, though there are some discrepancies from the end of August to middle September when the GEFS-Aerosols
30 underpredicts the high AOD episode (Figure 9b). GEFS-Aerosols is able to predict the two AOD enhancements in mid-October
31 and early November, which is quite comparable as ICAP. The correlation (RMSE) is 0.856 (0.15) and 0.936 (0.09) for GEFS-

Deleted: 1

1 Aerosols and ICAP with respect to AERONET at the site of Itajuba, only 0.451 (0.22) for NGACv2. The NGACv2 prediction
2 also generally underestimates the observations at this site too (Figure 9b). The NGACv2 results are closer to the ICAP, GEFS-
3 Aerosols and AERONET before August, and NGACv2 shows a slight increase of total AOD in early September, but the
4 NGACv2 AOD magnitude is much lower than the AERONET by about a factor of 5-7 from the middle of August onward.

5 Located in the southern part of the Amazon fire region, the site of Santa Cruz Utepsa is south of the AltaFloresta site. The
6 correlation (RMSE) values of GEFS-Aerosols and ICAP with respect to AERONET are 0.8 (0.18) and 0.88 (0.13)
7 respectively, which shows better performance than those of NGACv2 with 0.3 (0.39) at this site in predicting the total AOD
8 through the 5 months from July to November (Figure 9c). The model not only reproduces the total AOD temporal variation of
9 the AERONET results, but also captures several fluctuations of high AOD in August and September caused by Amazon fire
10 events. Again, some of fluctuations in total AOD were captured by the NGACv2 prediction, but the modeled AOD magnitudes
11 are 2-4 times lower than the observations.

12 The last site of RioBranco is also located in the Amazon fire source region but to the west of the AltaFloresta site. There are
13 some missing data at this site for the AERONET total AOD from middle July to middle September (Figure 9d). During this
14 period, the GEFS-Aerosols prediction is slightly lower than ICAP by about 5-10%. Both ICAP and GEFS-Aerosols total AOD
15 match the AERONET variations well when the AERONET data are available again from mid-September. Several peaks of
16 total AOD are also captured by GEFS-Aerosols in middle September and early November. The NGACv2 prediction shows
17 enhanced total AOD in middle August, with low biases by more than 2-3 times compared to ICAP and GEFS-Aerosols. For
18 other enhancements of total AOD after October, the NGACv2 results completely miss the fire events and do not show any
19 fluctuations. The correlation (RMSE) is 0.80 (0.24) and 0.90 (0.17) for GEFS-Aerosols and ICAP with respect to AERONET
20 at the site of RioBranco, only 0.51 (0.44) for NGACv2.

21 We also evaluate the total AOD time series of AERONET against ICAP, NGACv2 and GEFS-Aerosols for fire regions of
22 central and southern Africa. The comparisons at seven AERONET sites from July to November are shown in Figure
23 10. Generally, the GEFS-Aerosols predictions are able to capture the daily total AOD variation measured by AERONET. At
24 the site of Misampfu, the GEFS-Aerosols mode is somewhat better than that of ICAP in predicted the peaks of high AOD. The
25 correlation coefficients at the sites of [Ascension Island](#) and Lubango are much high than those of ICAP (see Table 1). While
26 both the GEFS-Aerosols and ICAP overpredicted the total AOD most of time throughout the three months at the station
27 Bamenda located north of the major African fire source region. The NGACv2 total AOD forecast shows under prediction at
28 most of the AERONET sites in this region. Meanwhile, NGACv2 and ICAP predictions are not consistent with AERONET
29 either, especially for several observed high peaks which are not reproduced by the model results (e.g. Gabon). At the remote
30 site of Ascension Island located west of the African fire source region, the GEFS-Aerosols and ICAP are able to capture the
31 AOD enhancements in the middle of August, and shows the best performance of the three different models (see Table 1). For
32 other sites that are located in the fire source region, such as Monguinn, Misamptu, Maun Tower, and Lubango, the prediction

Deleted: Maun Tower

1 of the GEFS-Aerosols model shows higher correlation of 0.68, 0.79, 0.84 and 0.71 than those of NGACv2 as 0.51, 0.26, 0.29,
2 0.35. The RMSE values of GEFS-Aerosols are 0.18, 0.15, 0.10, 0.15, which is much lower than the NGACv2 of 0.32, 0.34,
3 0.23, and 0.32. It suggests that the GEFS-Aerosols better matches the observed temporal variation of total AOD than NGACv2.
4 One peak in early August at the Monguinn site, one peak in middle September at the Misampfu site, two peaks in early August
5 and early September at Maun Tower site and one enhancement in August at Lubango are all predicted by the GEFS-Aerosols
6 model. The ICAP forecasts shows lower biases against the AERONET total AOD for predicting these peaks, while none of
7 these peaks are captured by NGACv2. GEFS-Aerosols shows slight over predictions in mid-July and late August for Gabon
8 and early August for Lubango.

9 **4.3 Evaluation of AOD associated with dust events**

10 Thirteen AERONET sites inside the major dust source regions of western North Africa, Asia and the Middle East and
11 surrounding areas have available data from July to November 2019. The total AOD time series of GEFS-Aerosols, ICAP, and
12 NGACv2 at 6 of these sites are shown in Figure 11. Overall, the GEFS-Aerosols model is able to closely predict the observed
13 total AOD variation, especially at the sites of Banizoumbu, Tenerife, Saada, Ben Salem, Granada and Sede Boker, with much
14 better performance than those of NGACv2 according to the correlation (RMSE) values in Table 1 of GEFS-Aerosols as 0.74
15 (0.15), 0.77 (0.07), 0.76 (0.14), 0.82 (0.07), 0.85 (0.09), and 0.73 (0.08) versus NGACv2 as 0.33 (0.24), 0.25 (0.18), 0.25
16 (0.26), 0.25 (0.23), 0.21 (0.16), and 0.19 (0.14). In addition to NGACv2's overprediction at the sites of Ben Salem and Granada,
17 it does not accurately capture observed temporal variations of total AOD at these sites.

18 We compare the daily AERONET total AOD with the 1-day forecasts of total AOD from GEFS-Aerosols and NGACv2 at the
19 AERONET sites of Cape Verde, Tamanrasset and Tenerife located in the dust source region over North Africa in Figure 12.
20 The slope of the linear regression of AERONET total AOD vs. GEFS-Aerosols is quite different from that of NGACv2 at the
21 site of Tamanrasset, which is located in southern Algeria and in the middle of the Saharan dust source region. The GEFS-
22 Aerosols linear regression slope is much closer to 1 than that of NGACv2, and the R^2 in the NGACv2 model is lower by a
23 factor of 4 than that of the GEFS-Aerosols model at this site. At the other two sites of Cape Verde and Tenerife, which are in
24 the downwind area west of the African dust source region, the slopes of the linear regressions for GEFS-Aerosols are also
25 much closer to 1 than those of the NGACv2 model. The NGACv2 model, as evidenced by the R^2 values, is more poorly
26 correlated with AERONET than the GEFS-Aerosols prediction. The R^2 values of GEFS-Aerosols is 0.50, 0.33 and 0.59 in
27 these sites, which better captures the dust transport in the downwind areas west of the African dust source region than the
28 NGACv2 model as 0.19, 0.08 and 0.06. [GEFS-Aerosols model is using FENGSH dust scheme, which is quite different to the](#)
29 [GOCART dust scheme using in NGACv2, which shows significant improvements in the dust AOD predictions.](#)

30 **4.4 Evaluation of major regional averages**

1 Figure 13 shows day 1 predictions of total AOD time series by GEFS-Aerosols and NGACv2 compared against the MERRA-
2 2 reanalysis averaged over 9 major global regions from August 2019 to March 2020. The comparison clearly shows the
3 consistency between GEFS-Aerosols and the MERRA-2 reanalysis over most of these 9 regions, especially North Africa, the
4 North Atlantic, Southern Africa, and the South Atlantic, with only minor discrepancies during these 8 months. The total AOD
5 is dominated by dust in North Africa and fire emissions in Southern Africa. The aerosols emitted from dust and fire regions
6 and their long-range transport play important roles in impacting the total AOD over the North and South Atlantic Oceans. The
7 good agreement with MERRA-2 shows that GEFS-Aerosols captures the emissions and transport of dust and fire emissions in
8 these regions.

9 Total AOD variation in South America is mainly related to biomass burning emissions. GEFS-Aerosols has some slight low
10 biases relative to MERRA-2 from middle September to early October 2019 that are associated with the Amazon fire event.
11 GEFS-Aerosols under predicts MERRA-2 in this region from mid-November 2019 to March 2020, outside the main biomass
12 burning season, which suggests that the GEFS-Aerosol AOD low biases in this region are mostly associated with sources other
13 than fires.

14 The European region has the largest differences between GEFS-Aerosols and MERRA-2 reanalysis total AOD among the 9
15 regions. Although their temporal variations are similar, GEFS-Aerosols under predicts the MERRA-2 total AOD throughout
16 the whole period by a factor of 0.5. The large absolute low biases from August to early October 2019 and March 2020 in
17 Europe which are associated with GEFS-Aerosols underestimates of sulfate AOD (Fig. 8).

18 From August to early December 2019, the GEFS-Aerosols total AOD looks quite consistent with the MERRA-2 reanalysis on
19 average across East Asia. GEFS-Aerosols high biases starting in middle December 2019 and increasing from January to March
20 2020 may be associated with the lockdown in China during the Coronavirus disease 2019 (COVID-19) pandemic.
21 Anthropogenic emissions of NO₂, SO₂, VOC, and primary PM_{2.5} over the North China Plain during this period were reduced
22 by 51%, 28%, 67% and 63%, respectively, compared to the previous year, resulting in lower surface aerosol and ozone levels
23 and improvements to air quality [Shi and Brasseur, 2020; Wang and Su, 2020; Xing et al., 2020]. Since the anthropogenic
24 emissions used in GEFS-Aerosols are based on the CEDS 2014 inventory, they definitely overestimate the anthropogenic
25 aerosol emissions during the 2019-2020 lockdown periods.

26 Both the Eastern and Western US regions exhibit GEFS-Aerosols low biases of about 5-30%, with the largest differences in
27 Eastern US occurring in August 2019. However, the trends of total AOD temporal variations with low in summer and high in
28 winter in the GEFS-Aerosols prediction and the MERRA-2 reanalysis are quite consistent over Eastern and Western US. The
29 minor under predictions by GEFS-Aerosols need further investigation.

30 In comparison, the NGACv2 predictions show significant under prediction of MERRA-2 total AOD for almost all of these 9
31 regions throughout this 8-month period. The one exception is North Africa, where the NGACv2 results are close to the
32 MERRA-2 reanalysis, with over prediction in August 2019 and low biases from December 2019 to March 2020. In addition

1 to its general under prediction of MERRA-2 total AOD, NGACv2 is not able to capture the temporal variations of total AOD
2 in some regions, such as the enhanced AOD due to fire emissions in Southern Africa, South Atlantic and South America.
3 Though NGACv2 shows similar temporal variations to MERRA-2 total AOD in Europe, East Asia, and the US, the magnitudes
4 of NGACv2 predictions are too low by a factor of 1 to 3. This analysis is consistent with a 1-year evaluation of GEFS-Aerosols
5 AOD that shows improvements over NGACv2 [Bhattacharjee et al., 2021]

6 5. ATom-1 retrospective forecast evaluation

7 Retrospective simulations of GEFS-Aerosols and NGACv2 were performed for the summer of 2016 and evaluated using
8 aircraft measurements from the first deployment of the Atmospheric Tomography Mission (ATom-1) in July and August 2021.
9 During ATom-1, plumes from dust storms and large biomass burning events and low-level sea salt aerosols were observed
10 over the southern and central Atlantic, and anthropogenic pollution was observed over the United States on the last flight from
11 Minnesota to Southern California.

12 In this section, we evaluate the 24-hour forecast skill of GEFS-Aerosols and NGACv2 by comparing with ATom-1
13 observations. The GEFS-Aerosols and NGACv2 model results are sampled at the same latitude, longitude and altitude as the
14 ATom-1 measurements. The model output is hourly with ~25km horizontal resolution on the FV3 native grid. The ATom-1
15 measurements collected on a 1-second time base were compared to the nearest hour's model forecast. Model data is
16 interpolated vertically (according to log-Z above ground level), but sampled within the nearest horizontal grid as the
17 observations (with no horizontal interpolation). Thus, the inherent differences between temporal (differences of up to 0.5 hour)
18 and spatial scales of the observations (~200 m resolution) and model results (25-100 km resolution) must be kept in mind with
19 the model-measurement comparisons.

20 5.1 Global flight track column sum comparisons

21 Figure 14 shows the tropospheric column sums of OC along the flight tracks of the NASA DC-8 for the ATom-1 observations
22 and GEFS-Aerosols model experiments. The OC column sums using GBBEPx v3 fire emissions at ~25 km resolution (Fig.
23 14 (b) are quite consistent and comparable to the observations. The modeled OC column sums are somewhat smaller than
24 those of observation over the north Atlantic, Greenland, and southeastern Canada.

25 Results of the model-measurement comparisons for dust are shown in Figure 15. GEFS-Aerosols simulations show good
26 agreement with ATom-1 observations over tropical north Atlantic and downwind of the western Africa dust source region.

27 However, the model underestimates the dust columns over tropical south Atlantic, Greenland, southeastern Canada, while
28 underestimating dust over the US, Alaska and broad areas of the Pacific Ocean. The GEFS-Aerosols model shows a clear
29 enhancement of the dust event sampled on 8/17/16 east of the African coastline near 22°N, though the model column maxima
30 tend to be more than a factor of 5 lower than the observations.

Deleted: V3

Deleted: overestimates

1 Table 3 gives median bias and correlation statistics for column sums of all GEFS-Aerosols model cases as well as the [NGACv2](#)
2 dust forecasts for ~130 profiles illustrated in Figures 14 and 15. Correlations (r – Pearson correlation coefficients) are typically
3 above 0.7 for all species except dust. The OC differences noted above for GBBEPx [v3](#) are apparent in the bias statistics of OC
4 (a factor of 2.5) and BC (a factor of 50%), although R-correlations are not significantly affected. Differences in the fire
5 inventories also affect sulfate biases slightly (12%). For all species except for dust, decreases in median model/observed ratios
6 are seen for the model results.

7 Dust, on the other hand, shows a slight underprediction in column amount in the model results. Dust sources depend critically
8 on surface wind speed, have very little overlap with the anthropogenic and biomass-burning sources of the other species, and
9 are associated with areas of weather and surface conditions, all which may contribute to the different response of dust emissions.
10 Correlations of dust are also much lower than for other species, and there is a very obviously difference between GEFS-
11 Aerosols and [NGACv2](#) model forecast statistics as discussed further below. We note that sea-salt columns are not calculated
12 or compared to ATom-1 observations, due to the large amount of observations below the detection limit, especially above 2
13 km altitude.

14 5.2 Vertical profile statistics comparisons

15 ATom-1 flight tracks are separated into 2 sections and labeled as the “Pacific” side for July 29 to August 8 2016 flights and
16 the “Atlantic” side for August 15 to August 23 2016 flights. For this analysis the 1-second model and observed data are binned
17 into 10 equally spaced vertical intervals (~1km) covering the vertical extent of the ATom-1 profiles. Figure 16 shows median,
18 ratio and correlation statistics of OC, BC and sulfate for the 2 geographic regions and the two model cases. For OC over the
19 Pacific, the median values are lower than that of the observation by more than 50%. Their correlations with observation are
20 quite similar above ~3 km height. The vertical profile of ratio also suggests that the OC concentrations are underpredicted over
21 Pacific. Statistics for the Atlantic flight tracks of ATom-1 show similar trends and behavior. The median values of model
22 prediction OC are quite comparable to observations, which show very consistent vertical variation similar to the observations.
23 The correlations with observations improve below 4 km height compared to those of the Pacific with the maximum closed to
24 0.80. While the correlations decrease significantly at 3-6 km height, it increases almost 50% above 6km height. The model
25 results are biased too low below ~3km. The BC vertical profile statistics are quite different to OC with the model forecasts
26 much larger than observations as one goes higher in altitude over both the Pacific and Atlantic section. Correlation coefficients
27 with observations are about 0.6-0.8 from near surface to ~ 6km over Pacific and about 0.7-0.9 below ~4km over Atlantic. The
28 correlations of both OC and BC decrease significantly above ~4km over the Atlantic. For sulfate, the median biases of model
29 are biased too low from near surface to ~ 8 km over the Pacific and their correlation coefficients with observations are about
30 0.4-0.6 below 6 km. For the Atlantic, median values are quite comparable to the observation below ~7 km and their correlations
31 are about 0.3~0.9 and consistently decreasing with altitude. By contrast, the Pacific comparisons for sulfate show a significant

Deleted: NGAC

Deleted: NGAC

1 underprediction (60-70%) from the 0.5 to 7.0 km altitude for both model cases, which suggests a significant underprediction
2 of oceanic gas-phase sulfur sources, such as DMS.
3 Vertically resolved statistics of naturally occurring dust and sea salt are shown in Figure 17. For dust over the Pacific, median
4 values of GEFS-Aerosols are too low while the NGACv2 results are too high compared with the observations, and the
5 correlations are almost less than 0.5. The performance of GEFS-Aerosols improves over the Atlantic with median values
6 comparable to observations above ~4km and the correlation coefficients increasing to 0.5~0.8 below ~5km. While it is still
7 showing a significant high bias for the NGACv2 model over Atlantic. For sea salt, the median values biases are all biased too
8 low over both the Pacific and Atlantic. Generally, the correlations are much better below ~6 km.

9 **5.3 Height-latitude profile comparisons over the Atlantic during ATom-1**

10 The ATom-1 flight profiles allow a more detailed comparison of aerosol spatial patterns from different aerosol sources with
11 the model. High values of OC and BC from fires were observed on 8/15/16 and 8/17/16 over the Atlantic, as were high values
12 of dust and sea-salt. The flight track of height-latitude profiles of OC, BC and sulfate for these combined days are shown in
13 Figure 18 for the ATom-1 measurements and the model results. The model results show similar pattern as the ATOM-1 in
14 reproducing the profiles of OC even using log scale, especially the biomass burning plumes near the tropics, though the model
15 results show slightly low biases. But they also show some bias for OC at levels above 4~5 km over the north Atlantic, where
16 model results show high biases. Overall, predicted BC (middle column of Figure 18) is able to capture the decreasing trend
17 with increasing altitude in the latitude-height profiles, however they are underpredicted in the biomass burning plumes near
18 the tropics from the surface to 5 km height in both model experiments, which have been seen in other models due to insufficient
19 wet scavenging [Wang et al., 2014, Choi et al., 2020]. Similar to the OC profiles, the model results overpredict above 4-5 km
20 height levels. It appears the model does not reproduce the enhancements of BC at 1-4 km height very well over this area. It
21 may be possibly due to relative weak convection or a low modeled injection height that the fire emission has not been lifted
22 enough to this altitude, which need further studies. For sulfate (right column), the model experiments show high concentrations
23 at low altitude, similar to the observations, though there are still some differences for the plume location at 2-4 km height that
24 shift the plume from near the equator to near 20°N in the model experiments. Over the equatorial areas at about 2-4 km height,
25 the observed sulfate concentration is underestimated by about 30% by modeled results, which may also relate to the injection
26 height of biomass burning those results in much lower SO₂ at this altitude since SO₂ is one of the important precursors for
27 sulfate production. Meanwhile, the sulfate concentration above 6 km is overestimated over the tropics while underestimated
28 near the surface.

29 Figure 19 shows the comparisons of the naturally occurring dust and sea salt aerosols for the same time period. In the left
30 column of dust, we also include the NGACv2 results. For more consistent comparisons, here the modeled dust results are
31 summed up by the first two bins to match the observation particle size range (less than 3 μm). The GEFS-Aerosol predictions

1 show agreement in the dust height-latitude profiles with the observations and exhibit similar patterns. The observed dust
2 plumes are reproduced by the model over 15-35°N, but the model appears to underestimate wet removal in the upper levels
3 that results in the overestimation of dust above 7-8 km height in northern Atlantic and above 5 km height in the tropical
4 southern Atlantic. On the other hand, the NGACv2 prediction shows a very large bias over broad areas of the north Atlantic
5 and the tropical southern Atlantic. A high dust plume near 35°S has not been captured well by the model from the surface to
6 the upper levels, which may be caused by missing dust events over South America. For sea salt, the model results are able to
7 predict patterns consistent with the observation, especially from the surface to about 4-6 km height.

8 6. Summary and future plan

9 Since the dynamical core of FV3 developed by GFDL has been selected by NOAA to be the dynamical core for the Next
10 Generation Global Prediction System (NGGPS), development of a coupled weather and atmospheric chemical composition
11 model for chemical weather and air quality forecasting based on the FV3 framework has begun couple of years ago. The
12 development as a single ensemble member of the Global Ensemble Forecast System (GEFS) has been completed. This new
13 model, referred to as GEFS-Aerosols, was implemented as one member of the GEFS into operations as part of NOAA's first
14 coupled UFS model in September 2020 and replaced previous operational global aerosol prediction system NGACv2 at NCEP.
15 The chemical component of atmospheric composition in GEFS-Aerosols is based on WRF-Chem, which is a community
16 modeling system used by thousands of users worldwide. The aerosol modules are based on modules from the GOCART model.
17 Features of the new model include: 1) the biomass burning plume rise module added from WRF-Chem; 2) the FENGSHA
18 dust scheme implemented and developed by NOAA Air Resources Laboratory (ARL); 3) all sub-grid scale tracer transport
19 and deposition is handled inside the physics routines requiring consistent implementation of positive definite tracer transport
20 and wet scavenging in the SAS scheme; 4) the updated background fields of OH, H₂O₂ and NO₃ from GMI model; 5) biomass-
21 burning emission calculations based on the GBBEPx v3 emission and FRP provided by NESDIS; and 6) global anthropogenic
22 emission inventories derived from CEDS and HTAP. These fundamental updates in GEFS-Aerosols indicate quite different
23 features compared to the NGACv2 (see Table 2), including dynamical core, physics package, coupling infrastructure,
24 horizontal resolution, and emission. These may play important roles in affecting the aerosol transport, wet and dry deposition,
25 and emission etc., which would help to improve the model performance. This new model is able to forecast the higher-
26 resolution distribution of primary air pollutants of aerosols: black carbon, organic carbon, sulfate, and dust and sea salt each
27 with five size bins. Meanwhile, it is also capable of handling volcanic eruptions, which can inject vast quantities of particulates
28 into the atmosphere. While for the predicted results in the paper, we have not included the volcanic emission into the model
29 for the June 2019 Raikoke eruption, it may partially impact on the underprediction over high northern latitude.
30 The updates in anthropogenic and fire emission indicate that the GEFS-Aerosols shows much better performance matching
31 the AOD observations when configured to use the CEDS anthropogenic emission and GBBEPx v3 fire emissions with plume-

Deleted: V3

Deleted: Several sensitivity experiments using different emissions inputs

Deleted: model

Deleted: the best

Deleted: V3

1 rise module [compared to NGACv2, especially over the fire source regions](#). For more extensive evaluation, we performed 9
2 months of Day-1 real-time forecast of GEFS-Aerosols starting in July 2019 and the predicted AOD was used to compare with
3 the satellite observations from MODIS and VIIRS, reanalysis data of ICAP-MME and MERRA-2, AERONET observations,
4 and the model predictions from MERRA-2 and NGACv2. Overall, GEFS-Aerosols [indicates](#) substantial improvement for both
5 composition and variability of aerosol distributions over those from the currently operational global aerosol prediction system
6 of NGACv2. Globally, the GEFS-Aerosols predicted biases with respect to MERRA-2 forecast for dust, OC and sulfate AOD
7 were improved compared to those from NGACv2. Substantial improvements were seen for the total AOD prediction when
8 compared with MERRA-2 reanalysis during the period of July to November 2019. Though there are still some high biases
9 over southern African fire region and eastern Asia and low biases over south America and dust source regions, GEFS-Aerosols
10 reproduces the prominent temporal and geographical features of AOD as represented by satellite observations and reanalysis
11 data, like dust plumes over North Africa and the Arabian Peninsula, biomass burning plumes in Southern Hemisphere, South
12 America, Northwestern America and Eastern Europe, polluted air over Eastern and Southern Asia, and high-altitude sea-salt
13 bands. We also sampled the forecast total AOD of GEFS-Aerosols and NGACv2 in the same location as 60 AERONET sites,
14 which are spread globally and represent different aerosol regimes, and compared their variations for the 7/5/19-11/30/19. Much
15 higher correlation coefficients against AERONET data are indicated for the GEFS-Aerosols than those for NGACv2 globally,
16 and are quite comparable to those of the ICAP-MME.

17 During the biomass burning events, GEFS-Aerosols captured major fires over southern Africa, Siberia, Central Amazon and
18 Central South America much better than NGACv2. Part of the improvement may be due to the vertical transport by the plume-
19 rise module. Generally, the total AOD time series of GEFS-Aerosols predictions matches closely to those of ICAP and
20 AERONET during most of the time from July to November 2019 at the AERONET sites over South America, except there
21 are some minor under predictions of several highest AOD episodes. In contrast, NGACv2 substantially underpredicted almost
22 throughout the whole period and almost entirely missed many high AOD events. For the southern African event, the GEFS-
23 Aerosols predictions are able to capture the daily total AOD variations seen in the AERONET observations, even better than
24 that of the ICAP total AOD at the sites near the fire source regions, though there are overpredictions at the sites in downwind
25 areas, which may be due to the lack of removal process or uncertainties of fire emission in central and southern Africa. In
26 contrast, the NGACv2 results show under prediction in total AOD forecast at most of the AERONET sites in this region.

27 Overall, the model predicts total AOD variation by GEFS-Aerosols indicates much better performance than that of NGACv2
28 over western North Africa. Although GEFS-Aerosols shows reductions in dust emissions over the Saharan dust source, the
29 correlations with observations from downwind AERONET sites in western Africa are improved over those for NGACv2. The
30 largest biases and discrepancies of GEFS-Aerosols and NGACv2 are both indicated in the sites in Tajikistan, which may be
31 associated with a missing dust source near this site for both models. [Obviously, other than the updates in anthropogenic and](#)
32 [fire emissions, the implementation of FENGSH dust scheme into GEFS-Aerosols also shows great improvements in the dust](#)

Deleted: is a

1 [concentration and AOD predictions over the dust regions compared to that of the NGACv2, which was using the original](#)
2 [GOCART dust scheme.](#)

3 We also evaluated predicted aerosols concentrations with different resolution against the ATom-1 aircraft measurements from
4 July to August 2016. Overall, predicted aerosol concentrations are quite comparable to the ATom-1 measurements along the
5 flight tracks globally with ~25 km model resolution. The model shows good performance in reproducing vertical profiles of
6 OC, BC, sulfate, dust and sea salt, and the location of fire plumes was captured well overall. Sulfate over the Pacific, southern
7 and tropical Atlantic is significantly underpredicted, suggesting an underestimation in the oceanic sulfur sources, such as DMS.
8 A clear trend in increased overprediction with altitude for BC suggests that further refinements in characterizing precipitation
9 scavenging of aerosol in GEFS-Aerosols is needed, since this is the only loss process for BC other than surface deposition.

10 [Compared to NGACv2, the much better performance of dust vertical profile at high latitude over Atlantic may suggest that](#)
11 [the dust removal processes \(either dry or wet deposition\) may be more accurate in GEFS-Aerosols. That may be partly](#)
12 [associated with different atmospheric model and physical scheme version using in GEFS-Aerosols. The differences in large](#)
13 [scale wet deposition and convective wet scavenging schemes between GEFS-Aerosols and NGACv2 may also contribute to](#)
14 [the substantial improvements showing in GEFS-Aerosols prediction for both AOD and concentrations.](#)

15 This paper overviews advances and challenges in model development for operational atmospheric aerosol predictions at
16 NOAA. This implementation advanced the global aerosol forecast capability for NOAA and made a step forward toward
17 developing a global aerosol data assimilation system. Currently, the assimilation of AOD based on satellite observations is
18 under development to constrain aerosol distributions in the GEFS-Aerosols model. Initial testing shows promise for
19 improvement of predictions as well as limitations indicating the need for refinements in quality control, data assimilation
20 impacts on aerosol composition and vertical distribution, as well as a need for bias correction of satellite observations. With
21 bias and other errors substantially reduced in the GEFS-Aerosols, especially when it is equipped with an aerosol data
22 assimilation system. Current, though the aerosol feedback from the aerosol components has not yet been included into the
23 atmospheric model for direct and indirect radiative feedback, the model provides a good starting point from which to
24 investigate at the impact on weather predictions out to sub-seasonal and seasonal scales when including the aerosol feedbacks
25 on atmospheric system in the future plan.

26 **Code and data availability**

27 The GEFS-Aerosols v1 code and model configuration for aerosol forecast here are available at
28 <https://doi.org/10.5281/zenodo.5655290>. ATom-1 data is publicly available at the Oak Ridge National Laboratory Distributed
29 Active Archive Center: https://daac.ornl.gov/ATOM/guides/ATOM_merge.html (Wofsy et al., 2018).

Deleted: and

1 **Author contribution**

2 Li Zhang and Raffaele Montuoro were the major developers of the GEFS-Aerosols model, including implementing and
3 coupling the aerosol components to the FV3GFSv15 meteorological model. Stuart McKeen helped to process the
4 anthropogenic emission and background input data, provided suggestions during the development of GEFS-Aerosols, and
5 evaluated the model performance with ATom-1 observations. Barry Baker developed and implemented the FENGSHA dust
6 scheme into GEFS-Aerosols. Partha Bhattacharjee helped to evaluate the GEFS-Aerosols real-time and operational predictions.
7 Georg Grell provided oversight of the model development. Li Zhang and Judy Henderson developed the workflow for GEFS-
8 Aerosols prediction and worked with Li Pan to perform and manage the real-time and retrospective forecasts. R. Ahmadov
9 provided guidance on the implementation of the fire plume rise scheme. Shobha Kondragunta, Xiaoyang Zhang, and Fangjun
10 Li provided the GBBEPx v3 data. The other co-authors provided help, suggestions and project management throughout the
11 GEFS-Aerosols modeling system development. Li Zhang prepared the manuscript with contributions from all co-authors.

Deleted: V3

12 **Competing interests**

13 The authors declare that they have no conflict of interest.

14 **Acknowledgements**

15 Li Zhang, Raffaele Montuoro, Haiqin Li and Ravan Ahmadov were supported by funding from NOAA GSL Award Number
16 NA17OAR4320101. This work was also supported by the UFS Research to Operations Medium Range Weather/Seasonal to
17 Subseasonal Atmospheric Composition sub-project.

18 **Reference**

19 Ahmadov R, Grell G, James E, Csiszar I, Tsidulko M, Pierce B, [McKeen, S., Benjamin, S., Alexander, C., Pereira, G., Freitas,](#)
20 [S., Goldberg, M.](#): Using VIIRS Fire Radiative Power data to simulate biomass burning emissions, plume rise and smoke
21 transport in a real-time air quality modeling system. 2017 Ieee International Geoscience and Remote Sensing Symposium.
22 IEEE International Symposium on Geoscience and Remote Sensing IGARSS. New York: Ieee; p. 2806-8, 2017.

23 Bauer, S. E., Im, U., Mezuman, K., & Gao, C. Y.: Desert dust, industrialization, and agricultural fires: Health impacts of
24 outdoor air pollution in Africa. [Journal of Geophysical Research: Atmospheres](#), 124, 4104–4120,
25 <https://doi.org/10.1029/2018JD029336>, 2019.

26 [Benedetti, A., Reid, J.S. and Colarco, P.R.:](#) [International cooperative for aerosol prediction workshop on aerosol forecast](#)
27 [verification](#). [Bulletin of the American Meteorological Society](#), 92, ES48–ES53. <https://doi.org/10.1175/BAMS-D-11-00105.1>,
28 [2011](#).

Deleted: et al.

Deleted:

Deleted:

Deleted:

Deleted:

Deleted:

Deleted:

Deleted:

Deleted:

Deleted:

1 Bhattacharjee, P. S., Wang, J., Lu, C.-H., and Tallapragada, V.: The implementation of NEMS GFS Aerosol Component
2 (NGAC) Version 2.0 for global multispecies forecasting at NOAA/NCEP – Part 2: Evaluation of aerosol optical thickness,
3 Geosci. Model Dev., 11, 2333–2351, <https://doi.org/10.5194/gmd-11-2333-2018>, 2018.

4 Bhattacharjee, P. S., Zhang, L., Baker, B., Pan, L., Montuoro, R., Grell A. G., and McQueen, J. Evaluation of Aerosol Optical
5 Depth forecast from NOAA's Global Aerosol Forecast Model (GEFS-Aerosols). To be submitted. 2021.

6 Black, T. L., Abeles, J. A., Blake, B. T., Jovic, D., Rogers, E., Zhang, X., Aligo, E. A., Dawson, L. C., Lin, Y., Strobach, E.,
7 Shafran, P. C., Carley, J. R.: A limited area modeling capability for the Finite-Volume Cubed-Sphere (FV3) dynamical core
8 and comparison with a global two-way nest. *Journal of Advances in Modeling Earth Systems*, 13,
9 e2021MS002483. <https://doi.org/10.1029/2021MS002483>, 2021.

10 Bloom, S., Silva, A. da, and Dee, D.: *Documentation and validation of the Goddard Earth Observing System (GEOS) data*
11 *assimilation system-version 4*, 1–187 pp, 2005.

12 Bourgeois, I., Peischl, J., Thompson, C. R., Aikin, K. C., Campos, T., Clark, H., Commane, R., Daube, B., Diskin, G. W.,
13 Elkins, J. W., Gao, R.-S., Gaudel, A., Hints, E. J., Johnson, B. J., Kivi, R., McKain, K., Moore, F. L., Parrish, D. D., Querel,
14 R., Ray, E., Sánchez, R., Sweeney, C., Tarasick, D. W., Thompson, A. M., Thouret, V., Witte, J. C., Wofsy, S. C., and Ryerson,
15 T. B.: Global-scale distribution of ozone in the remote troposphere from the ATom and HIPPO airborne field missions, *Atmos.*
16 *Chem. Phys.*, 20, 10611–10635, <https://doi.org/10.5194/acp-20-10611-2020>, 2020.

17 Bozzo, A., Benedetti, A., Flemming, J., Kipling, Z., and Rémy, S.: An aerosol climatology for global models based on the
18 tropospheric aerosol scheme in the Integrated Forecasting System of ECMWF, *Geosci. Model Dev.*, 13, 1007–1034,
19 <https://doi.org/10.5194/gmd-13-1007-2020>, 2020.

20 Burnett, R., Chen, H., Szyszczkiewicz, M., Fann, N., Hubbell, B., Pope, C. A., Spte, J.S., Brauer, M., Cohen, A., Weichenthal,
21 S., Coggins, J., Di, Q., Brunekreef, B., Frostad, F., Lim, S.S., Kan, H., Walker, K.d., Thurston, G.D., Hayes, R.b., Lim, C.C.,
22 Turner, M. C., Jerrett, M., Krewski, D., Gapstur, S.M., Diver, W.R., Ostro, B., Goldberg, D., Crouse, D.L., Martin, R.V.,
23 Peters, P., Pinault, L., Tjepkema, M., Donkelaar, A., Villeneuve, P.J., Miller, A.B., Yin, P., Zhou, M., Wang, L., Janssen
24 N.A.H., Marra, M., Atkinson, R.W., Tsang, H., Thach, T.Q., Cannon, J.B., Allen, R.T., Hart, J.E., Laden, F., Cesaroni, G.,
25 Forastiere, F., Weinmayr, G., Jaensch, A., Nagel, G., Concin, H., and Spadaro, J.V.: Global estimates of mortality associated
26 with longterm exposure to outdoor fine particulate matter, *P. Natl. Acad. Sci. USA*, 115(38), 9592–9597,
27 doi:10.1073/pnas.1803222115, 2018.

28 Chappell, A., and Webb, N. P.: Using albedo to reform wind erosion modelling, mapping and monitoring. *Aeolian Research*,
29 23, 63–78. <https://doi.org/10.1016/j.aeolia.2016.09.006>, 2016.

30 Chen, J. M., Li, C. L., Ristovski, Z., Milic, A., Gu, Y. T., Islam, M. S., Wang, S. X., Hao, J. M., Zhang, H. F., He, C. R., Guo,
31 H., Fu, H. B., Miljevic, B., Morawska, L., Thai, P., Fat, L., Pereira, G., Ding, A. J., Huang, X., and Dumka, U. C.: A review
32 of biomass burning: Emissions and impacts on air quality, health and climate in China, *Sci. Total Environ.*, 579, 1000–
33 1034, <https://doi.org/10.1016/j.scitotenv.2016.11.025>, 2017.

34 Chen, Q., Yin, Y., Jin, L.-J., Xiao, H., Zhu, S.-Ch.: The effect of aerosol layers on convective cloud microphysics and
35 precipitation, *Atmos. Res.*, 101 (1-2), pp. 327–340 <http://doi.org/10.1016/j.atmosres.2011.03.007>, 2011.

36 Chin, M., Ginoux, P., Kinne, S., Torres, O., Holben, B., Duncan, B., Martin, R., Logan, J., Higurashi, A., and Nakajima, T.:
37 Tropospheric aerosol optical thickness from the GOCART model and comparisons with satellite and Sun photometer
38 measurements, *J. Atmos. Sci.*, 59, 461–483, 2002.

39 ~~Chin, M., Rood, B. R., Lin, S.-J., Muller, F. J., and Thomson, M. A.: Atmospheric sulfur cycle in the global model GOCART:
40 Model description and global properties, *J. Geophys. Res.*, 105, 24,671–24,687, 2000.~~

41 Choi, Y., Kanaya, Y., Takigawa, M., Zhu, C., Park, S.-M., Matsuki, A., Sadanaga, Y., Kim, S.-W., Pan, X., and Pizzo, I.:
42 Investigation of the wet removal rate of black carbon in East Asia: validation of a below- and in-cloud wet removal scheme in

Deleted:

Deleted:

Deleted:

Deleted:

Deleted:

Deleted:

Deleted:

Deleted:

Deleted:

Moved down [2]: Rood, B. R., Lin, S.-J., Muller, F. J., and Thomson, M. A.: Atmospheric sulfur cycle in the global model GOCART:

Deleted: Model description and global properties, J.

Moved down [3]: *Geophys. Res.*, 105, 24,671–24,687, 2000.

Deleted: ¶

Moved down [4]: Chin, M.,

Moved (insertion) [4]

Moved (insertion) [2]

Moved (insertion) [3]

1 FLEXible PARTicle (FLEXPART) model v10.4, *Atmos. Chem. Phys.*, 20, 13655–13670, [https://doi.org/10.5194/acp-20-](https://doi.org/10.5194/acp-20-13655-2020)
2 13655-2020, 2020.

3 Colarco, P. R., Kahn, R. A., Remer, L. A., and Levy, R. C.: Impact of satellite viewing-swath width on global and regional
4 aerosol optical thickness statistics and trends, *Atmos. Meas. Tech.*, 7, 2313–2335, <https://doi.org/10.5194/amt-7-2313-2014>,
5 2014.

6 Colarco, P., [Benedetti, A.](#), [Reid, J.](#) and [Tanaka, T.](#): [Using EOS data to improve aerosol forecasting: the International](#)
7 [Cooperative for Aerosol Research \(ICAP\)](#). *The Earth Observer*, 26, 14–19, 2014.

8 [Colarco, P.](#), [da Silva, A.](#), [Chin, M.](#), and [Diehl, T.](#): [Online simulations of global aerosol distributions in the NASA GEOS-4](#)
9 [model and comparisons to satellite and ground-based aerosol optical depth](#). *J. Geophys. Res.*, 115, D14207,
10 doi:[10.1029/2009JD012820](https://doi.org/10.1029/2009JD012820), 2010.

11 Darmenov, A. and da Silva, A.: The Quick Fire Emissions Dataset (QFED) – Documentation of versions 2.1, 2.2 and 2.4,
12 NASA Technical Report Series on Global Modeling and Data As- simulation, NASA/TM-2015–104606, Vol. 38, 211 pp.,
13 avail- able at: <http://citeseerx.ist.psu.edu/viewdoc/download?doi=10.1.1.406.7724&rep=rep1&type=pdf> (last access: 4 June
14 2018), 2015.

15 Diehl, T., Heil, A., Chin, M., Pan, X., Streets, D., Schultz, M., and Kinne, S.: Anthropogenic, biomass burning, and volcanic
16 emis- sions of black carbon, organic carbon, and SO₂ from 1980 to 2010 for hindcast model experiments, *Atmos. Chem. Phys.*
17 *Dis- cuss.*, 12, 24895–24954, <https://doi.org/10.5194/acpd-12-24895-2012>, 2012.

18 Easter, R. C., Ghan, S. J., Zhang, Y., Saylor, R. D., Chapman, E. G., Laulainen, N. S., Abdul-Razzak, H., Leung, L. R., Bian,
19 X., and Zaveri, R. A.: MIRAGE: Model Description and Evaluation of Aerosols and Trace Gases. *J. Geophys. Res.*, 109,
20 D20210, doi:[10.1029/2004JD004571](https://doi.org/10.1029/2004JD004571), 2004.

21 Eck, T. F., Holben, B. N., Reid, J. S., Dubovik, O., Smirnov, A., O'Neill, N. T., Slutsker, I., and Kinne, S.: The wavelength
22 dependence of the optical depth of biomass burning, urban and desert dust aerosols, *J. Geophys. Res.*, 104, 31333–31350,
23 1999.

24 Fast, J. D., Gustafson Jr., I. W., Easter, C. R., Zaveri, A. R., Barnard, C. J., Chapman, G. E., Grell, A. G., and Peckham, E. S.:
25 Evolution of ozone, particulates, and aerosol direct radiative forcing in the vicinity of Houston using a fully coupled
26 meteorology-chemistry-aerosol model. *J. Geophys. Res.*, 111, D21305, doi:[10.1029/2005JD006721](https://doi.org/10.1029/2005JD006721), 2006.

27 Fécán, F., Marticorena, B. and Bergametti, G.: Parametrization of the increase of the aeolian erosion threshold wind friction
28 velocity due to soil moisture for arid and semi-arid areas. *Annales Geophysicae*, 17, 149–157, [https://doi.org/10.1007/s00585-](https://doi.org/10.1007/s00585-999-0149-7)
29 999-0149-7, 1998.

30 Flentje, H., Mattis, I., Kipling, Z., Rémy, S., and Thomas, W.: Evaluation of ECMWF IFS-AER (CAMS) operational forecasts
31 during cycle 41r1–46r1 with calibrated ceilometer profiles over Germany, *Geosci. Model Dev.*, 14, 1721–1751,
32 <https://doi.org/10.5194/gmd-14-1721-2021>, 2021.

33 Forkel, R., Werhahn, J., Buus Hansen, A., McKeen, S., Peckham, S., Grell, G., Suppan, P.: Effect of aerosol-radiation feedback
34 on regional air qualityeacase study with WFR/Chem. *Atmos. Environ.* 53,
35 202e211.<http://dx.doi.org/10.1016/j.atmosenv.2011.10.009>, 2012

36 Freitas, S. R., Longo, K. M., Alonso, M. F., Pirre, M., Marecal, V., Grell, G., Stockler, R., Mello, R. F., and Sánchez Gácita,
37 M.: PREP-CHEM-SRC – 1.0: a preprocessor of trace gas and aerosol emission fields for regional and global atmospheric
38 chemistry models, *Geosci. Model Dev.*, 4, 419–433, doi:[10.5194/gmd-4-419-2011](https://doi.org/10.5194/gmd-4-419-2011), 2011.

39 Freitas, S. R., Longo, K. M., Chatfield, R., Latham, D., Silva Dias, M. A. F., Andreae, M. O., Prins, E., Santos, J. C., Gielow,
40 R., and Carvalho Jr., J. A.: Including the sub-grid scale plume rise of vegetation fires in low resolution atmospheric transport
41 models, *Atmos. Chem. Phys.*, 7, 3385–3398, <https://doi.org/10.5194/acp-7-3385-2007>, 2007.

Deleted:

Deleted:

Deleted:

Deleted:

Deleted:

Deleted:

Deleted: 10.1029/2009JD012820

Formatted: Pattern: Clear

Formatted: Pattern: Clear

Formatted: Pattern: Clear

Deleted:

Formatted: Pattern: Clear

Deleted:

Formatted: Pattern: Clear

Deleted:

Formatted: Pattern: Clear

Formatted: Pattern: Clear

1 Froyd, K. D., Murphy, D. M., Brock, C. A., Campuzano-Jost, P., Dibb, J. E., Jimenez, J.-L., Kupc, A., Middlebrook, A. M.,
2 Schill, G. P., Thornhill, K. L., Williamson, C. J., Wilson, J. C., and Ziemba, L. D.: A new method to quantify mineral dust and
3 other aerosol species from aircraft platforms using single-particle mass spectrometry, *Atmos. Meas. Tech.*, 12, 6209–6239,
4 <https://doi.org/10.5194/amt-12-6209-2019>, 2019.

5 Gelaro, R., McCarty, W., Suárez, M. J., Todling, R., Molod, A., Takacs, L., Randles, C. A., Darmenov, A., Bosilovich, M. G.,
6 Reichle, R., Wargan, K., Coy, L., Cullather, R., Draper, C., Akella, S., Buchard, V., Conaty, A., da Silva, A. M., Gu, W., Kim,
7 G., Koster, R., Lucchesi, D., Merkova, J. E., Nielsen, G., Partyka, G., Pawson, S., Putman, W., Rienecker, M., Schubert, S. D.,
8 Sienkiewicz, M., and Zhao, B.: The Modern-Era Retrospective Analysis for Research and Applications, Version 2 (MERRA-
9 2), *J. Climate*, 30, 5419–5454, <https://doi.org/10.1175/JCLI-D-16-0758.1>, 2017.

10 Gillette, D. A., Adams, J., Endo, A., Smith, D., and Kihl, R.: Threshold velocities for input of soil particles into the air by
11 desert soils, *J. Geophys. Res.*, 85(C10), 5621–5630, doi:10.1029/JC085iC10p05621, 1980.

12 Gillette, D. A.: Threshold friction velocities for dust production for agricultural soils. *Journal of Geophysical Research*,
13 93(D10), 12645–12662. <https://doi.org/10.1029/jd093id10p12645>, 1988.

14 Grell, G. A., Peckham, E. S., Schmitz, R., McKeen, A. S., Frost, G., Skamarock, W., and Eder, B.: Fully-coupled online
15 chemistry within the WRF model. *Atmospheric Environment*, 39, 6957–6975, doi:10.1016/j.atmosenv.2005.04.027, 2005.

16 Grell, G., Freitas, S. R., Stuefer, M., and Fast, J.: Inclusion of biomass burning in WRF-Chem: impact of wildfires on weather
17 forecasts, *Atmos. Chem. Phys.*, 11, 5289–5303, <https://doi.org/10.5194/acp-11-5289-2011>, 2011.

18 Hoesly, R. M., Smith, S. J., Feng, L., Klimont, Z., Janssens-Maenhout, G., Pitkanen, T., Seibert, J. J., Vu, L., Andres, R. J.,
19 Bolt, R. M., Bond, T. C., Dawidowski, L., Kholod, N., Kurokawa, J.-I., Li, M., Liu, L., Lu, Z., Moura, M. C. P., O'Rourke, P.
20 R., and Zhang, Q.: Historical (1750–2014) anthropogenic emissions of reactive gases and aerosols from the Community
21 Emissions Data System (CEDS), *Geosci. Model Dev.*, 11, 369–408, <https://doi.org/10.5194/gmd-11-369-2018>, 2018.

22 Holben, B. N., Eck, T. F., Slutsker, I., Tanré, D., Buis, J. P., Setzer, A., Vermote, E., Reagan, J. A., Kaufman, Y. J., Nakajima,
23 T., Lavenu, F., Jankowiak, I., and Smirnov, A.: AERONET – A Federated instrument network and data archive for aerosol
24 characterization, *Remote Sens. Environ.*, 66, 1–16, 1998.

25 Hollingsworth, A., Engelen, R. J., Textor, C., Benedetti, A., Boucher, O., Chevallier, F., Dethof, A., Elbern, H., Eskes, H.,
26 Flemming, J., Granier, C., Kaiser, J. W., Morcrette, J.-J., Rayner, P., Peuch, V.-H., Rouil, L., Schultz, M. G., and Simmons,
27 A. J.: Toward a Monitoring and Forecasting System For Atmospheric Composition: The GEMS Project, *B. Am. Meteorol.*
28 *Soc.*, 89, 1147–1164, 2008.

29 Hsu, N. C., Jeong, M.-J., Bettenhausen, C., Sayer, A. M., Hansell, R., Seftor, C. S., Huang, J., and Tsay, S.-C.: Enhanced Deep
30 Blue aerosol retrieval algorithm: The second generation, *J. Geophys. Res.-Atmos.*, 118, 9296–
31 9315, <https://doi.org/10.1002/jgrd.50712>, 2013.

32 Jackson, J., Liu, H., Laszlo, I., Kondragunta, S., Remer, L. A., Huang, J., and Huang, H.-C.: Suomi-NPP VIIRS Aerosol
33 Algorithms and Data Products, *J. Geophys. Res.*, 118, 12673–12689, <https://doi.org/10.1002/2013jd020449>, 2013.

34 Janssens-Maenhout, G., Crippa, M., Guizzardi, D., Dentener, F., Muntean, M., Pouliot, G., Keating, T., Zhang, Q., Kurokawa,
35 J., Wankmüller, R., Denier van der Gon, H., Kuenen, J. J. P., Klimont, Z., Frost, G., Darras, S., Koffi, B., and Li, M.:
36 HTAP_v2.2: a mosaic of regional and global emission grid maps for 2008 and 2010 to study hemispheric transport of air
37 pollution, *Atmos. Chem. Phys.*, 15, 11411–11432, <https://doi.org/10.5194/acp-15-11411-2015>, 2015.

38 Janssens-Maenhout, G.: EDGARv4.1 Emission Time Series, European Commission, Joint Research Centre (JRC) [Dataset]
39 PID, available at: <http://data.europa.eu/89h/jrc-edgar-emissiontimeseriesv41>, (last access: 12 June 2018), 2010.

40 Levin, Z., and Cotton R. W.: *Aerosol Pollution Impact on Precipitation*, Aerosol Pollution Impact on Precipitation: A Scientific
41 Review, 407 pp., Springer, New York, 2009.

Formatted: Pattern: Clear

Deleted:

Deleted:

Deleted: .

Formatted: Pattern: Clear

Formatted

(... [1])

Deleted: ...Adams, J., ...Endo, A., ...Smith, D., and ...Kihl, R.: ...Threshold velocities for input of soil particles into the air by desert soils, ...*J. Geophys. Res.*, ...85(C10), ...5621–

(... [2])

Formatted: Pattern: Clear

Formatted: pb_toc_link

Deleted: Hausteine, K., Pérez, C., Baldasano, J. M., Jorba, O., Basart, S., Miller, R. L., Janjic, Z., Black, T., Nickovic, S., Todd, M. C., Washington, R., Müller, D., Tesche, M., Weinzierl, B., Esselborn, M., and Schladitz, A.: Atmospheric dust modeling from meso to global scales with the online NMMB/BSC-Dust model – Part 2: Experimental campaigns in Northern Africa, *Atmos. Chem. Phys.*, 12, 2933–2958, <https://doi.org/10.5194/acp-12-2933-2012>, 2012. Hoesly et al,

Formatted: pb_toc_link, Font color: Auto

Deleted:).

Formatted: pb_toc_link, Font color: Auto

Deleted: .

Deleted: -

Formatted: pb_toc_link, Font color: Auto

Formatted

(... [3])

Formatted

(... [4])

Deleted: .

Moved (insertion) [5]

Formatted

(... [5])

Deleted: .

Formatted: Pattern: Clear

Deleted:

Formatted

(... [6])

Deleted: .

Formatted: Pattern: Clear

Formatted

(... [7])

1 Levy, R. C., Mattoo, S., Munchak, L. A., Remer, L. A., Sayer, A. M., Patadia, F., and Hsu, N. C.: The Collection 6 MODIS
2 aerosol products over land and ocean, *Atmos. Meas. Tech.*, 6, 2989–3034, <https://doi.org/10.5194/amt-6-2989-2013>, 2013.

3 Liu, F., Zhang, Q., van der A, R. J., Zheng, B., Tong, D., Yan, L., Zheng, Y., and He, K.: Recent reduction in NO_x emissions
4 over China: synthesis of satellite observations and emission inventories, *Environ. Res. Lett.*, 11,
5 114002, <https://doi.org/10.1088/1748-9326/11/11/114002>, 2016.

6 Liu, H., Remer, L. A., Huang, J., Huang, H.-C., Kondragunta, S., Laszlo, I., Oo, M., and Jackson, J. M.: Preliminary Evaluation
7 of Suomi-NPP VIIRS Aerosol Optical Thickness, *J. Geophys. Res.*, 119, 3942–3962, <https://doi.org/10.1002/2013jd020360>,
8 2013.

9 Lu, C.-H., da Silva, A., Wang, J., Moorthi, S., Chin, M., Colarco, P., Tang, Y., Bhattacharjee, P. S., Chen, S.-P., Chuang, H.-
10 Y., Juang, H.-M. H., McQueen, J., and Iredell, M.: The implementation of NEMS GFS Aerosol Component (NGAC) Version
11 1.0 for global dust forecasting at NOAA/NCEP, *Geosci. Model Dev.*, 9, 1905–1919, <https://doi.org/10.5194/gmd-9-1905-2016>,
12 2016.

13 Lu, S., Huang, H.-C., Hou, Y.-T., Tang, Y., McQueen, J., da Silva, A., Chin, M., Joseph, E., and Stockwell, W.: Development
14 of NCEP Global Aerosol Forecasting System: an overview and its application for improving weather and air quality forecasts,
15 in: *NATO Science for Peace and Security Series: Air Pollution Modelling and Its Application XX*, Springer Publications,
16 Dordrecht, the Netherlands, 451–454, <https://doi.org/10.1007/978-90-481-3812-8>, 2010.

17 MacKinnon, D. J., Clow, G. D., Tigges, R. K., Reynolds, R. L., and Chaves Jr, P. S.: Comparison of aerodynamically and
18 model-derived roughness lengths (z_0) over diverse surfaces, central Mojave Desert, California, USA, *Geomorphology*, 63,
19 103–113, doi:10.1016/j.geomorph.2004.03.009, 2004

20 Marticorena, B. and Bergametti, G.: Modeling the atmospheric dust cycle: 1-Design of a soil derived dust production scheme,
21 *J. Geophys. Res.*, 100, 16415-16430, 1995.

22 Molod, A., Takacs, L., Suarez, M., and Bacmeister, J.: Development of the GEOS-5 atmospheric general circulation model:
23 evolution from MERRA to MERRA2, *Geosci. Model Dev.*, 8, 1339–1356, <https://doi.org/10.5194/gmd-8-1339-2015>, 2015.

24 Morcrette, J.-J., Beljaars, A., Benedetti, A., Jones, L. and Boucher, O.: Sea-salt and dust aerosols in the ECMWF IFS model,
25 *Geophysical Research Letters*, 35, L24813, 2008.

26 Muhlbauer, A., Grabowski, W. W., Malinowski, P. S., Ackerman, P. T., Bryan, H. G., Lebo, J. Z., Milbrandt, A. J., Morrison,
27 H., Ovchinnikov, M., Tessendorf, S., Thériault, G. J.M.: Thompson Reexamination of the state of the art of cloud modelling
28 shows real improvements, *Bull. Am. Meteorol. Soc.*, 94, pp. ES45–ES48, <http://doi.org/10.1175/BAMS-D-12-00188.1>, 2013.

29 Mulcahy, J. P., Walters, D. N., Bellouin, N., and Milton, S. F.: Impacts of increasing the aerosol complexity in the Met Office
30 global numerical weather prediction model, *Atmos. Chem. Phys.*, 14, 4749–4778, doi:10.5194/acp-14-4749-2014, 2014.

31 Murphy, D. M., Froyd, K. D., Bian, H., Brock, C. A., Dibb, J. E., DiGangi, J. P., Diskin, G., Dollner, M., Kupc, A., Scheuer,
32 E. M., Schill, G. P., Weinzierl, B., Williamson, C. J., and Yu, P.: The distribution of sea-salt aerosol in the global troposphere,
33 *Atmos. Chem. Phys.*, 19, 4093–4104, <https://doi.org/10.5194/acp-19-4093-2019>, 2019.

34 Murphy, D., Froyd, K., Apel, E., Blake, R. D., Blake, J. N., Evangelioiu, N., Hornbrook, S. R., Peischl, J., Ray, E., Ryerson, B.
35 T., Thompson, C., and Stohl, A.: An aerosol particle containing enriched uranium encountered in the remote T upper
36 troposphere, *J. Environ. Radioactivity*, 184–185, 95-100, doi:10.1016/j.jenvrad.2018.01.006, 2018

37 Owen, P. R.: Saltation of uniform grains in air. *Journal of Fluid Mechanics*, 20(2), 225–242.
38 <https://doi.org/10.1017/S0022112064001173>, 1964.

39 Powers, J. G., Klemp, J. B., Skamarock, W. C., Davis, C. A., Dudhia, J., Gill, D. O., Coen, J. L., Gochis, D. J., Ahmadov, R.,
40 Peckham, S. E., Grell, G. A., Michalakes, J., Trahan, S., Benjamin, S. G., Alexander, C. R., Dimego, G. J., Wang, W., Schwartz,
41 C. S., Romine, G. S., Liu, Z., Snyder, C., Chen, F., Barlage, M. J., Yu, W., & Duda, M. G. : The Weather Research and

Deleted:

Formatted: Pattern: Clear

Deleted: .

Formatted: Pattern: Clear

Formatted: Pattern: Clear

Formatted: Pattern: Clear

Formatted: Pattern: Clear

Formatted: Pattern: Clear

Deleted: .

Formatted: Pattern: Clear

Deleted:

Formatted: Pattern: Clear

Deleted:

Formatted: Pattern: Clear

Deleted:

Formatted: Pattern: Clear

Deleted:

Formatted: Pattern: Clear

Deleted:

Formatted: Pattern: Clear

Deleted:

Formatted: Pattern: Clear

Deleted:

Formatted: Pattern: Clear

Deleted:

Formatted: Pattern: Clear

Deleted:

Formatted: Pattern: Clear

Deleted:

Formatted: Pattern: Clear

Deleted:

Formatted: Pattern: Clear

1 Forecasting Model: Overview, System Efforts, and Future Directions, *Bulletin of the American Meteorological Society* 98(8),
2 1717-1737, 2017.

3 Prigent, C., Jiménez, C., and Catherinot, J.: Comparison of satellite microwave backscattering (ASCAT) and visible/near-
4 infrared reflectances (PARASOL) for the estimation of aeolian aerodynamic roughness length in arid and semi-arid regions,
5 *Atmos. Meas. Tech.*, 5, 2703–2712, <https://doi.org/10.5194/amt-5-2703-2012>, 2012.

6 Raupach, M. R.: Drag and drag partition on rough surfaces. *Boundary-Layer Meteorology*.
7 <https://doi.org/10.1007/BF00155203>, 1992.

8 Reale, O., Lau, K. M., and Silva da, A.: Impact of interactive aerosol on the African easterly jet in the NASA GEOS-5 Global
9 Forecasting System. *Wea. Forecasting*, 26, 504–519, 2011.

10 Reid, J., Benedetti, A., Colarco, P. R., and Hansen, J. A.: International operational aerosol observability work-shop, *B. Am.*
11 *Meteorol. Soc.*, 92, ES21-ES24, <https://doi.org/10.1175/2010BAMS3183.1>, 2011.

12 Rienecker, M.M., Suarez, M.J., Todling, R., Bacmeister, J., Takacs, L., Liu, H.-C., Gu, W., Sienkiewicz, M., Koster, R.D.,
13 Gelaro, R., Stajner, I. and Nielsen, J.E.: *The GEOS-5 data assimilation system: documentation of versions 5.0.1, 5.1.0, and*
14 *5.2.0*, Suarez, M.J. (ed.). NASA Tech. Memo. 2008-104606, Vol. 27, 2008.

15 Rodwell, M. J. and Jung, T.: Understanding the local and global impacts of model physics changes: an aerosol example, *Q.J.R.*
16 *Meteorol. Soc.*, 134, 1479–1497, doi:10.1002/qj.298, 2008.

17 Sayer, A. M., Hsu, N. C., Bettenhausen, C., and Jeong, M.-J.: Validation and uncertainty estimates for MODIS Collection 6
18 “Deep Blue” aerosol data, *J. Geophys. Res.-Atmos.*, 118, 7864–7872, <https://doi.org/10.1002/jgrd.50600>, 2013.

19 Sayer, A. M., Munchak, L. A., Hsu, N. C., Levy, R. C., Bettenhausen, C., and Jeong M.-J.: MODIS Collection 6 aerosol
20 products: Comparison between Aqua’s e-Deep blue, dark target and “merged” data sets and usage recommendations,
21 *J. Geophys. Res.-Atmos.*, 119, 13965–989, 2014.

22 Schill, G.P., Froyd, K.D., Bian, H., Kupc, A., Williamson, C., Brock, C. A., Ray, E., Hornbrook, R. S., Hills, A. J., Apel, E.
23 C., Chin, M., Colarco, P. R., Murphy, D. M.: Widespread biomass burning smoke throughout the remote troposphere. *Nat.*
24 *Geosci.* 13, 422–4. <https://doi.org/10.1038/s41561-020-0586-1>, 2020

25 Sessions, W. R., Reid, J. S., Benedetti, A., Colarco, P. R., da Silva, A., Lu, S., Sekiyama, T., Tanaka, T. Y., Baldasano, J. M.,
26 Basart, S., Brooks, M. E., Eck, T. F., Iredell, M., Hansen, J. A., Jorba, O. C., Juang, H.-M. H., Lynch, P., Morcrette, J.-J.,
27 Moorthi, S., Mulcahy, J., Pradhan, Y., Razingar, M., Sampson, C. B., Wang, J., and Westphal, D. L.: Development towards a
28 global operational aerosol consensus: basic climatological characteristics of the International Cooperative for Aerosol
29 Prediction Multi-Model Ensemble (ICAP-MME), *Atmos. Chem. Phys.*, 15, 335–362, [https://doi.org/10.5194/acp-15-335-](https://doi.org/10.5194/acp-15-335-2015)
30 [2015](https://doi.org/10.5194/acp-15-335-2015), 2015.

31 Shao, Y., Jshizuka, M., Mikami, M., and Leys, J. F.: Parameterization of size-resolved dust emission and validation with
32 measurements. *Journal of Geophysical Research Atmospheres*, 116(8), D08203. <https://doi.org/10.1029/2010JD014527>, 2011.

33 Shao, Y., Raupach, M. R., and Findlater, P. A.: Effect of saltation bombardment on the entrainment of dust by wind. *Journal*
34 *of Geophysical Research*, 98(D7), 12719–12726. <https://doi.org/10.1029/93jd00396>, 1993.

35 Shi, X., and Brasseur, G. P.: The response in air quality to the reduction of Chinese economic activities during the COVID-19
36 outbreak. *Geophysical Research Letters*, 47, e2020GL088807, <https://doi.org/10.1029/2020GL088807>, 2020.

37 Slinn, W. G. N.: Precipitation scavenging, in *Atmospheric Science and Power Production*, edited by: D. Randerson, U.S. Dept.
38 of Energy, Washington D. C., 472–477, 1984.

39 Theurich, G., DeLuca, C., Campbell, T., Liu, F., Saint, K., Vertenstein, M., Chen, J., Oehmke, R., Doyle, J., Whitcomb, T.,
40 Wallcraft, A., Iredell, M., Black, T., da Silva, A.M., Clune, T., Ferraro, R., Li, P., Kelley, M., Aleinov, I., Balaji, V., Zadeh,
41 N., Jacob, R., Kirtman, B., Giraldo, F., McCarren, D., Sandgathe, S., Peckham, S., and Dunlap, IV, R.: The Earth System

Deleted:
Formatted: Pattern: Clear

Deleted:
Formatted: Pattern: Clear

Formatted: Pattern: Clear

Formatted: Pattern: Clear

Formatted: Pattern: Clear

Formatted: Pattern: Clear

Deleted: Rosenfeld, D., Woodley, W. L., Khain, A., Cotton, W. R., Carrió, G., Ginis, I., and Golden, J. H.: Aerosol... [8]

Moved up [5]: Am. Meteorol. Soc

Deleted: . 93, 987–1001, 2012.¶

Formatted: Pattern: Clear

Formatted: Pattern: Clear

Formatted: Pattern: Clear

Formatted: Pattern: Clear

Formatted: Pattern: Clear

Formatted: Pattern: Clear

Deleted: .

Deleted: . et al.

Formatted: Pattern: Clear

Deleted:

Formatted: Pattern: Clear

Formatted: Pattern: Clear

Formatted: Pattern: Clear

Formatted: Pattern: Clear

Moved (insertion) [6]

Moved (insertion) [7]

Moved up [7]: Shao, Y.,

Moved up [6]: Ishizuka, M., Mikami, M., and Leys, J. F.:

Deleted:

Deleted:

Deleted:

Deleted:

Deleted:

Formatted: Pattern: Clear

1 Prediction Suite: Toward a coordinated U.S. modeling capability. *Bull. Amer. Meteorol. Soc.*, 97, no. 7, 1229-1247,
2 doi:10.1175/BAMS-D-14-00164.1, 2016.

3 Thomson, D.S., Schein, M. E., Murphy, D.M.: Particle analysis by laser mass spectrometry WB-57F instrument overview.
4 *Aero. Sci. Technol.* 33, 153–169, 2000.

5 Tong, D. Q., Wang, J. X. L., Gill, T. E., Lei, H., and Wang, B.: Intensified dust storm activity and Valley fever infection in
6 the southwestern United States. *Geophys. Res. Lett.* 44, 4304–4312, doi:10.1002/2017GL073524, 2017.

7 Wang, Q., Su M.: A preliminary assessment of the impact of COVID-19 on environment—a case study of China. *Sci Total*
8 *Environ.* 728:138915. doi: 10.1016/j.scitotenv.2020.138915. 2020.

9 Wang, H., Rasch, J. P., Easter, C. R., Singh, B., Zhang, R., Ma, P.-L., Qian, Y., Ghan, J. S., and Beagley, N.: Using an explicit
10 emission tagging method in global modeling of source receptor relationships for black carbon in the Arctic: Variations, sources,
11 and transport pathways. *J. Geophys. Res. Atmos.*, 119, 12,888–12,909, doi:10.1002/2014JD022297, 2014.

12 Wang, J., Bhattacharjee, P. S., Tallapragada, V., Lu, C.-H., Kondragunta, S., da Silva, A., Zhang, X., Chen, S.-P., Wei, S.-W.,
13 Darnenov, A. S., McQueen, J., Lee, P., Koner, P., and Harris, A.: The implementation of NEMS GFS Aerosol Component
14 (NGAC) Version 2.0 for global multispecies forecasting at NOAA/NCEP – Part 1: Model descriptions, *Geosci. Model Dev.*,
15 11, 2315–2332, <https://doi.org/10.5194/gmd-11-2315-2018>, 2018.

16 Wang, Q., Jacob, J. D., Spackman, R. J., Perring, E. A., Schwarz, P. J., Moteki, N., Marais, A. E., Ge, C., Wang, J., and Barrett,
17 R. H. S.: Global budget and radiative forcing of black carbon aerosol: Constraints from pole-to-pole (HIPPO) observations
18 across the Pacific. *J. Geophys. Res. Atmos.*, 119, 195–206, doi:10.1002/2013JD020824, 2014.

19 Wofsy, S. C., Afshar, S., Allen, H. M., Apel, E., Asher, E. C., Barletta, B., Bent, J., Bian, H., Biggs, B. C., Blake, D. R., Blake,
20 N., Bourgeois, I., Brock, C. A., Brune, W. H., Budney, J. W., Bui, T. P., Butler, A., Campuzano-Jost, P., Chang, C. S., Chin,
21 M., Commane, R., Correa, G., Crouse, J. D., Cullis, P. D., Daube, B. C., Day, D. A., Dean-Day, J. M., Dibb, J. E., Di-Gangi,
22 J. P., Diskin, G. S., Dollner, M., Elkins, J. W., Erdesz, F., Fiore, A. M., Flynn, C. M., Froyd, K., Gesler, D. W., Hall, S. R.,
23 Hanisco, T. F., Hannun, R. A., Hills, A. J., Hints, E. J., Hoffman, A., Hornbrook, R. S., Huey, L. G., Hughes, S., Jimenez, J.
24 L., Johnson, B. J., Katicich, J. M., Keeling, R. F., Kim, M. J., Kupc, A., Lait, L. R., Lamarque, J.-F., Liu, J., McKain, K.,
25 McLaughlin, R. J., Meinardi, S., Miller, D. O., Montzka, S. A., Moore, F. L., Morgan, E. J., Murphy, D. M., Murray, L. T.,
26 Nault, B. A., Neuman, J. A., Newman, P. A., Nicely, J. M., Pan, X., Paplawsky, W., Peischl, J., Prather, M. J., Price, D. J.,
27 Ray, E., Reeves, J. M., Richardson, M., Rollins, A. W., Rosenlof, K. H., Ryerson, T. B., Scheuer, E., Schill, G. P., Schroder,
28 J. C., Schwarz, J. P., St.Clair, J. M., Steenrod, S. D., Stephens, B. B., Strode, S. A., Sweeney, C., Tanner, D., Teng, A. P.,
29 Thames, A. B., Thompson, C. R., Ullmann, K., Veres, P. R., Vieznor, N., Wagner, N. L., Watt, A., Weber, R., Weinzierl, B.,
30 Wennberg, P., Williamson, C. J., Wilson, J. C., Wolfe, G. M., Woods, C. T., and Zeng, L. H.: ATom: Merged Atmospheric
31 Chemistry, Trace Gases, and Aerosols, ORNL DAAC, Oak Ridge, Tennessee, <https://doi.org/10.3334/orlnl/1581>, 2018.

32 Xian, P., Reid, J. S., Hyer, E. J., Sampson, C. R., Rubin, J. I., Ades, M., Asencio, N., Basart, S., Benedetti, A., Bhattacharjee,
33 P. S., Brooks, M. E., Colarco, P. R., da Silva, A. M., Eck, T. F., Guth, J., Jorba, O. I., Kouznetsov, R., Kipling, Z., Sofiev, M.,
34 Garcia-Pando, C. P., Pradhan, Y., Tanaka, T., Wang, J., Westphal, D. L., Yumimoto, K., Zhang, J.: Current state of the global
35 operational aerosol multi-model ensemble: An update from the International Cooperative for Aerosol Prediction (ICAP). *Q. J. R. Meteorol. Soc.*, 145, (Suppl. 1), 176–209, <https://doi.org/10.1002/qj.3497>, 2019.

36

37 Xie, S. P., B. Lu, and Xiang, Q. B.: Similar spatial patterns of climate responses to aerosol and greenhouse gas changes. *Nat.*
38 *Geosci.*, 6, 828–832, doi:<https://doi.org/10.1038/ngeo1931>, 2013.

39 Xing, J., Li, S., Jiang, Y., Wang, S., Ding, D., Dong, Z., Zhu, Y., and Hao, J.: Quantifying the emission changes and associated
40 air quality impacts during the COVID-19 pandemic on the North China Plain: a response modeling study. *Atmos. Chem. Phys.*,
41 20, 14347–14359, <https://doi.org/10.5194/acp-20-14347-2020>, 2020.

42 Yang, Q., Bitz, C. M., and Doherty, S. J.: Offsetting effects of aerosols on Arctic and global climate in the late 20th century,
43 *Atmos. Chem. Phys.*, 14, 3969-3975, <https://doi.org/10.5194/acp-14-3969-2014>, 2014.

Deleted:

Deleted:

Deleted:

Deleted:

Deleted:

Deleted:

Deleted:

Deleted:

Deleted:

Deleted:

Deleted:

Deleted:

Deleted:

Deleted:

Deleted:

Deleted:

Moved (insertion) [8]

Moved up [8]: Wang Q, Su M.: A preliminary assessment of the impact of COVID-19 on environment—a case study of China. *Sci Total Environ*, 728:138915. doi: 10.1016/j.scitotenv.2020.138915. 2020.

Formatted: pb_toe_link, Font color: Auto, Pattern: Clear

Deleted: Reid, J. S., Hyer, E. J. et al.

Formatted: pb_toe_link, Font color: Auto, Pattern: Clear

Deleted:

Formatted: pb_toe_link, Font color: Auto, Pattern: Clear

Formatted: pb_toe_link, Font color: Auto, Pattern: Clear

Formatted: pb_toe_link, Font color: Auto, Pattern: Clear

Formatted: pb_toe_link, Font color: Auto, Pattern: Clear

Formatted: pb_toe_link, Font color: Auto, Pattern: Clear

Formatted: pb_toe_link, Font color: Auto, Pattern: Clear

Deleted: ..

Formatted: pb_toe_link, Font color: Auto, Pattern: Clear

Deleted: (

Formatted: pb_toe_link, Font color: Auto, Pattern: Clear

Deleted:

Formatted: pb_toe_link, Font color: Auto, Pattern: Clear

Deleted:

Formatted: pb_toe_link, Font color: Auto, Pattern: Clear

Deleted: <https://doi.org/10.1002/qj.3497>,

Formatted: pb_toe_link, Font color: Auto

Formatted: Font color: Auto

Deleted: <https://doi.org/10.1038/ngeo1931>

Zhang, L., Grell, G. A., McKeen, S. A., Ahmadov, R., Froyd, K. D., and Murphy, D.: Inline coupling of simple and complex chemistry modules within the global weather forecast model FIM (FIM-Chem v1), *Geosci. Model Dev.*, 15, 467–491, <https://doi.org/10.5194/gmd-15-467-2022>, 2022.

Zhang, Q., He, K., and Huo, H.: Cleaning China's air, *Nature*, 484, 161–162, <https://doi.org/10.1038/484161a>, 2012.

Zhang, X., Kondragunta, S., da Silva, A., Lu, S., Ding, H., Li, F., and Zhu, Y.: The blended global biomass burning emissions product from MODIS and geostationary satellites (GBBEPx), http://www.ospo.noaa.gov/Products/land/gbbepx/docs/GBBEPx_ATBD.pdf (last access: 1 June 2018), 2014.

Zhang, X., Kondragunta, S., Ram, J., Schmidt, C., and Huang, H.-C.: Near-real-time global biomass burning emissions product from geostationary satellite constellation, *J. Geophys. Res.*, 117, D14201, <https://doi.org/10.1029/2012JD017459>, 2012.

Zhao, T. X., Stowe, L. L., Smirnov, A., Crosby, D., Sapper, J., and McClain, C. R.: Development of a global validation package for satellite oceanic aerosol optical thickness retrieval based on AERONET observations and its application to NOAA/NESDIS operational aerosol retrievals, *J. Atmos. Sci.*, 59, 294–312, 2002.

Table.

Table 1. AERONET site information, the correlation coefficients and root mean square error (RMSE) of GEFS-Aerosols, ICAP and NGACv2 AOD with respect to that of AERONET observation for the period 7/5/2019-11/30/2019. Correlation coefficients are at the 95% confidence interval.

Stations	Station Names	(Latitude, Longitude)	Corr. with GEFS-Aerosols	Corr. with NGACv2	Corr. with ICAP	RMSE with GEFS-Aerosols	RMSE with NGACv2	RMSE with ICAP
1	Dakar	(14.39N, 16.95W)	0.60	0.21	0.78	0.19	0.24	0.10
2	Cape Verde	(16.73N, 22.93W)	0.54	0.39	0.86	0.25	0.27	0.11
3	Banizoumbu	(13.54N, 2.66E)	0.46	0.23	0.81	0.19	0.25	0.14
4	Tamanrasset	(22.79N, 5.53E)	0.40	0.29	0.78	0.26	0.34	0.17
5	Tenerife	(28.47N, 16.24W)	0.55	0.32	0.88	0.17	0.19	0.06
6	Saada	(31.62N, 8.15W)	0.72	0.17	0.83	0.19	0.30	0.10
7	Ben Salem	(35.55N, 9.91E)	0.74	0.15	0.86	0.08	0.29	0.07
8	Sede Boker	(30.85N, 34.78E)	0.72	0.16	0.83	0.10	0.20	0.07
9	Dewa	(24.76N, 55.36E)	0.47	0.41	0.85	0.29	0.30	0.13
10	Granada	(37.16N, 3.60W)	0.82	0.32	0.77	0.08	0.13	0.08
11	Cape San Juan	(18.38N, 65.62W)	0.43	0.28	0.64	0.14	0.21	0.04
12	Dushanbe	(38.55N, 68.85E)	0.29	0.14	0.60	0.32	0.33	0.25
13	Dalanzadgaad	(43.57N, 104.41E)	0.71	0.46	0.81	0.13	0.16	0.10
14	Beijing	(39.97N, 116.38E)	0.67	0.47	0.80	0.43	0.68	0.33
15	Kanpur	(26.51N, 80.23E)	0.76	0.15	0.87	0.36	0.51	0.32
16	Kyiv	(50.36N, 30.49E)	0.45	0.18	0.62	0.14	0.20	0.06
17	Barcelona	(41.38N, 2.11E)	0.62	0.39	0.76	0.12	0.16	0.08
18	Leipzig	(51.35N, 12.43E)	0.77	0.20	0.80	0.11	0.13	0.05
19	Sochengcho	(37.42N, 124.73E)	0.63	0.63	0.74	0.31	0.47	0.24
20	Singapore	(1.29N, 103.78E)	0.40	0.19	0.62	0.66	0.89	0.36
21	Reunion St Denis	(20.90S, 55.48E)	0.42	0.46	0.74	0.05	0.08	0.05
22	Lumbini	(27.50N, 83.28E)	0.44	0.32	0.58	0.28	0.29	0.29
23	Cape Fuguei	(25.29N, 121.53E)	0.66	0.33	0.63	0.37	0.66	0.34
24	Lake Argyle	(16.10S, 128.74E)	0.60	0.37	0.78	0.06	0.06	0.05
25	Chilbolton	(51.14N, 1.43W)	0.66	0.20	0.79	0.09	0.12	0.05

Deleted:

Deleted: C., Liu, X., Leung, L. R., Johnson, B., McFarlane, S. A., Gustafson Jr., W. I., Fast, J. D., and Easter, R.: The spatial distribution of mineral dust and its shortwave radiative forcing over North Africa: modeling sensitivities to dust emissions and aerosol size treatments, *Atmos. Ch* (... [9])

Formatted: Font color: Auto

Formatted: Font color: Auto, Pattern: Clear

Deleted:

Formatted: Font color: Auto, Pattern: Clear

Deleted: .

Formatted: Font color: Auto, Pattern: Clear

Deleted: [10]

Formatted Table

Formatted: Pattern: Clear

Formatted: Pattern: Clear

Formatted: Pattern: Clear

Formatted: Pattern: Clear

Formatted: Pattern: Clear

Formatted: Pattern: Clear

Formatted: Pattern: Clear

Formatted: Pattern: Clear

Formatted: Pattern: Clear

Formatted: Pattern: Clear

Formatted: Pattern: Clear

Formatted: Pattern: Clear

Formatted: Pattern: Clear

Formatted: Pattern: Clear

Formatted: Pattern: Clear

Formatted: Pattern: Clear

Formatted: Pattern: Clear

Formatted: Pattern: Clear

Formatted: Pattern: Clear

Formatted: Pattern: Clear

Formatted: Pattern: Clear

Formatted: Pattern: Clear

26	Opal	(79.99N, 85.93W)	0.19	0.13	0.61	0.12	0.16	0.08
27	Resolute Bay	(74.70N, 94.96W)	0.28	0.21	0.62	0.11	0.11	0.06
28	Thule	(76.51N, 68.76W)	0.32	0.13	0.57	0.12	0.13	0.07
29	Kangerlussuaq	(66.99N, 50.62W)	0.83	0.35	0.97	0.09	0.10	0.05
30	Tomsk	(56.45N, 85.04E)	0.72	0.18	0.83	0.55	0.79	0.27
31	Hornsund	(77.0N, 15.54E)	0.66	0.68	0.90	0.13	0.16	0.07
32	Alta Floresta	(9.87S, 56.10W)	0.81	0.30	0.88	0.24	0.34	0.12
33	Santa Cruz Utepsa	(17.76S, 63.20W)	0.86	0.45	0.94	0.21	0.42	0.13
34	Itajuba	(22.41S, 45.45W)	0.43	0.25	0.57	0.17	0.24	0.09
35	La Paz	(16.53S, 68.06W)	0.48	0.19	0.79	0.07	0.12	0.08
36	SEGS Lope Gabon	(0.202S, 11.60E)	0.71	0.43	0.94	0.29	0.69	0.39
37	Ascension Island	(7.97S, 14.41W)	0.54	0.45	0.33	0.13	0.25	0.08
38	Bamenda	(5.94N, 10.15E)	0.67	0.59	0.94	0.17	0.17	0.47
39	Mongu Inn	(15.26S, 23.13E)	0.72	0.15	0.86	0.17	0.32	0.17
40	Misamfu	(10.17S, 31.22E)	0.80	0.38	0.83	0.17	0.35	0.15
41	Maun Tower	(19.9S, 23.55E)	0.66	0.26	0.85	0.10	0.22	0.11
42	Windpoort	(19.36S, 15.48E)	0.64	0.33	0.69	0.18	0.29	0.09
43	Lubango	(14.95S, 13.44E)	0.81	0.72	0.54	0.16	0.32	0.14
44	Bonanza Creek	(64.74N,148.31W)	0.77	0.21	0.70	0.32	0.60	0.23
45	Fort McMurray	(56.75N,111.47W)	0.72	0.14	0.71	0.16	0.29	0.12
46	Chapais	(49.82N, 74.97W)	0.32	0.11	0.55	0.11	0.14	0.07
47	Saturn Island	(48.77N,123.12W)	0.63	0.28	0.76	0.09	0.09	0.05
48	Missoula	(46.91N,114.08W)	0.43	0.14	0.79	0.09	0.11	0.04
49	Camaguey	(21.42N, 77.85W)	0.63	0.16	0.82	0.06	0.12	0.04
50	Neon Wood	(47.12N, 99.24W)	0.58	0.18	0.75	0.10	0.16	0.06
51	GSFC	(38.99N, 76.84W)	0.47	0.15	0.77	0.08	0.16	0.06
52	Monterey	(36.59N,121.85W)	0.39	0.32	0.66	0.04	0.04	0.03
53	Toronto	(43.79N, 79.47W)	0.66	0.17	0.52	0.15	0.19	0.10
54	Red Mountain Pass	(37.90N,107.71W)	0.65	0.15	0.76	0.03	0.04	0.02
55	Tucson	(32.23N,110.95W)	0.62	0.16	0.81	0.05	0.08	0.03
56	Appalachian State	(36.21N, 81.69W)	0.69	0.11	0.75	0.07	0.13	0.05
57	Cartel	(45.38N, 71.93W)	0.08	0.19	0.26	0.09	0.13	0.06
58	Mauna Loa	(19.53N,155.57W)	0.35	0.20	0.79	0.05	0.04	0.04
59	ARM SGP	(36.6N, 97.48W)	0.64	0.26	0.64	0.08	0.14	0.05
60	Univ. of Wisconsin	(43.07N, 89.41W)	0.60	0.21	0.78	0.06	0.08	0.05

Formatted: Pattern: Clear

Formatted: Pattern: Clear

Formatted: Pattern: Clear

Formatted: Pattern: Clear

Formatted: Pattern: Clear

Formatted: Pattern: Clear

Formatted: Pattern: Clear

Formatted: Pattern: Clear

Formatted: Pattern: Clear

Formatted: Pattern: Clear

Formatted: Pattern: Clear

Formatted: Pattern: Clear

Formatted: Pattern: Clear

Formatted: Pattern: Clear

Formatted: Pattern: Clear

Formatted: Pattern: Clear

Formatted: Pattern: Clear

Formatted: Pattern: Clear

Formatted: Pattern: Clear

Formatted: Pattern: Clear

Formatted: Pattern: Clear

Formatted: Pattern: Clear

Formatted: Pattern: Clear

Formatted: Pattern: Clear

Formatted: Pattern: Clear

Formatted: Pattern: Clear

Formatted: Pattern: Clear

Formatted: Pattern: Clear

Formatted: Pattern: Clear

Formatted: Pattern: Clear

Formatted: Pattern: Clear

Formatted: Pattern: Clear

Formatted: Pattern: Clear

Formatted: Pattern: Clear

Formatted: Pattern: Clear

Formatted: Pattern: Clear

Formatted: Pattern: Clear

Formatted: Pattern: Clear

Formatted: Pattern: Clear

Formatted: Pattern: Clear

Formatted: Pattern: Clear

Formatted: Pattern: Clear

Formatted: Pattern: Clear

Formatted: Pattern: Clear

Formatted: Pattern: Clear

Formatted: Pattern: Clear

Formatted: Pattern: Clear

Formatted: Pattern: Clear

Formatted: Pattern: Clear

Formatted: Pattern: Clear

Formatted Table

1
2
3
4

5 Table 2. Comparison of model configurations between GEFS-Aerosols and NGACv2

Mode Configurations	GEFS-Aerosols	NGACv2
Atmospheric model	FV3	NEMS GSM
Physics package	GFS v15 (2019)	GFS v2015 (2015)
Horizontal resolution	~25 km	~100 km
Vertical resolution	64 layers	64 layers
Coupled infrastructure	NUOPC	ESMF
Anthropogenic Emission	CEDS 2014	EDGAR v4.1

Fire Emission	GBBEPx v3	GBBEPx [Zhang et al., 2014]
Aerosol scheme for BC, OC, sulfate and sea salt	GOCART from WRF-Chem	GOCART from GEOS-5
Dust scheme	FENGSHA	GOCART

Deleted: and QFED v2

Table 3. A Tom-1 and GEFS-Aerosols column sum statistics of mean bias and correlation for sulfate, OC, EC and dust.

Species	N	Obs. median (mg/m ²)	GEFS-Aerosols	NGACv2	GEFS-Aerosols	NGACv2
			MMO	MMO	r-coefficient	r-coefficient
Sulfate	153	0.58	0.72	-	0.63	-
OC	146	0.55	1.03	-	0.80	-
BC	152	0.011	3.35	-	0.78	-
Dust (< 3. μm diam)	130	0.038	0.54	46.37	0.39	0.39

Deleted: FV3-C384

Deleted: NGAC-v2

Deleted: FV3-C384

Deleted: NGAC-v2

Formatted Table

Deleted: coeff.

Formatted: Left, Indent: Left: 0", First line: 0"

Deleted: coeff.

Deleted: Organic Carbon

Deleted: Elemental Carbon

Deleted: coeff.

Deleted:

N is the sample number, MMO stands for Median Model to Observed Ratio, and r-coefficient is the Pearson correlation r-coefficient.

Figure Captions.

Figure 1. Diagram showing the components within the NEMS infrastructure.

Deleted: GSDCHEM component

Figure 2. (a) Diagram of GEFS-Aerosols coupled structure; (b) Flowchart of steps/tasks for GEFS-Aerosols in the global workflow forecast system.

Figure 3. Anthropogenic emissions of CEDS (2014) and HTAP (2010) for SO₂ (mole/km²/hr), BC and OC (ng/m²/s) on summer of July.

Figure 4. Total AOD forecast on 25th August compared with the NGACv2 model, MERRA2 reanalysis data and satellite observations of VIIRS and MODIS. The 18z forecasts from both models for that day and daily satellite data are used in the figure. Satellite data gaps are in white.

Deleted: NGAC

Figure 5. Correlation coefficients and RMSE between AERONET daily total AOD observations and GEFS-Aerosols, ICAP and NGACv2 for the period 7/5/19-11/30/19. Correlation coefficients are at the 95% confidence interval.

Deleted: NGAC

Figure 6. Day 1 AOD prediction averaged during 7/5/19-11/30/19 of GEFS-Aerosols and NGACv2 compared with MERRA-2 reanalysis and MODIS.

Deleted: NGAC

Figure 7. Day 1 AOD forecast biases of GEFS-Aerosols and NGACv2 compared with MERRA-2 averaged during 7/5/19-11/30/19 for dust, OC and sulfate.

Deleted: NGAC

1 **Figure 8.** Differences of GEFS-Aerosols and [NGACv2](#) Day 1 predictions of total AOD compared with MERRA-2 reanalysis
2 averaged during 7/5/19-11/30/19.

3 **Figure 9.** Day 1 AOD forecasts of GEFS-Aerosols, ICAP, and [NGACv2](#) verified against AERONET sites in South America
4 during 7/5/19-11/30/19.

5 **Figure 10.** Day 1 AOD forecasts of GEFS-Aerosols, ICAP, and [NGACv2](#) verified against AERONET sites in Africa during
6 7/5/19-11/30/19.

7 **Figure 11.** Day 1 AOD forecasts of GEFS-Aerosols, ICAP, and [NGACv2](#) verified against AERONET sites in dust source
8 regions and surrounding downwind areas during 7/5/19-11/30/19.

9 **Figure 12.** Daily AERONET total AOD versus modeled total AOD from GEFS-Aerosols (blue) and [NGACv2](#) (orange) at the
10 AERONET sites of (a) Tamanrasset, (b) Cape Verde, and (c) Tenerife with linear regression fits.

11 **Figure 13.** GEFS-Aerosols and [NGACv2](#) day 1 total AOD forecast time series against MERRA-2 reanalysis data averaged
12 over major global regions of North Africa (0°-35°N, 18°W-30°E), North Atlantic Ocean, (0°-40°N, 10°-80°W), Southern
13 Africa (0°-35°S, 8°-35°E), South Atlantic (0°-35°S, 40°W-20°E), South America (0°-35°S, 35°W-80°W), Europe (35°-65°N,
14 10°W-50°E), East Asia (20°-48°N, 100°-140°E), Eastern USA (25°-48°N, 68°-95°W), and Western USA (25°- 48°N, 95°-
15 125°W).

16 **Figure 14.** Tropospheric column sums of OC (<1.0 μm diameter) for (a) [ATom-1](#) DC-8 observations; and (b) GEFS-Aerosols.

17 **Figure 15.** Tropospheric column sums of dust (<3.0 μm diameter) for (a) [ATom-1](#) DC-8 observations; (b) GEFS-Aerosols;
18 and (c) [NGACv2](#).

19 **Figure 16.** Vertically resolved statistical comparisons of median values (black line is [ATom-1](#) observation, red line is GEFS-
20 Aerosols), r-coefficient, and median ratio (model/observation) for OC, BC and sulfate along the [ATom-1](#) DC-8 flight tracks
21 over the Pacific (July 29-August 8) and Atlantic (August 15-23).

22 **Figure 17.** Vertically resolved statistical comparisons of median values (black line is [ATom-1](#) observation, red line is GEFS-
23 Aerosols, green line is [NGACv2](#)), r-coefficient, and median ratio (model/observation) for dust and sea salt along the [ATom-1](#)
24 DC-8 flight tracks over the Pacific (July 29-August 8) and Atlantic (August 15-23).

25 **Figure 18.** Height-latitude profiles of OC, BC and sulfate over Atlantic on August 15 and 17th, 2016 for (a) the [ATom-1](#) DC-
26 8 observations; (b) GEFS-Aerosols.

27 **Figure 19.** Height-latitude profiles of dust (<3.0 μm diameter) and sea salt (<3.0 μm diameter) over Atlantic on August 15
28 and 17th, 2016 for (a) the [ATom-1](#) DC-8 observations; (b) GEFS-Aerosols and (c) [NGACv2](#).

Deleted: NGAC

Deleted: NGAC

Deleted: NGAC

Deleted: NGAC

Deleted: NGAC

Deleted: NGAC

Deleted: NASA

Deleted: the NASA

Deleted: NGAC

Deleted: for

Deleted: Red line is with GEFS-Aerosols.

Deleted: for

Deleted: Red line is GEFS-Aerosols, green line is NGAC.

Deleted: EC

Deleted: NGAC

Page 30: [1] Formatted kate 5/24/22 5:04:00 PM

Pattern: Clear

Page 30: [1] Formatted kate 5/24/22 5:04:00 PM

Pattern: Clear

Page 30: [1] Formatted kate 5/24/22 5:04:00 PM

Pattern: Clear

Page 30: [2] Deleted kate 5/24/22 5:04:00 PM

▼

Page 30: [2] Deleted kate 5/24/22 5:04:00 PM

▼

Page 30: [2] Deleted kate 5/24/22 5:04:00 PM

▼

Page 30: [2] Deleted kate 5/24/22 5:04:00 PM

▼

Page 30: [2] Deleted kate 5/24/22 5:04:00 PM

▼

Page 30: [2] Deleted kate 5/24/22 5:04:00 PM

▼

Page 30: [2] Deleted kate 5/24/22 5:04:00 PM

▼

Page 30: [2] Deleted kate 5/24/22 5:04:00 PM

▼

Page 30: [2] Deleted kate 5/24/22 5:04:00 PM

▼

Page 30: [2] Deleted kate 5/24/22 5:04:00 PM

▼

Page 30: [3] Formatted kate 5/24/22 5:04:00 PM

pb_toc_link, Font color: Auto

Page 30: [3] Formatted kate 5/24/22 5:04:00 PM

pb_toc_link, Font color: Auto

Page 30: [4] Formatted kate 5/24/22 5:04:00 PM

pb_toc_link, Pattern: Clear

Page 30: [4] Formatted kate 5/24/22 5:04:00 PM

pb_toc_link, Pattern: Clear

▼

Page 30: [5] Formatted kate 5/24/22 5:04:00 PM

Pattern: Clear

Page 30: [5] Formatted kate 5/24/22 5:04:00 PM

Pattern: Clear

Page 30: [5] Formatted kate 5/24/22 5:04:00 PM

Pattern: Clear

Page 30: [5] Formatted kate 5/24/22 5:04:00 PM

Pattern: Clear

Page 30: [6] Formatted kate 5/24/22 5:04:00 PM

Pattern: Clear

Page 30: [6] Formatted kate 5/24/22 5:04:00 PM

Pattern: Clear

Page 30: [6] Formatted kate 5/24/22 5:04:00 PM

Pattern: Clear

Page 30: [7] Formatted kate 5/24/22 5:04:00 PM

Pattern: Clear

Page 30: [7] Formatted kate 5/24/22 5:04:00 PM

Pattern: Clear

Page 30: [7] Formatted kate 5/24/22 5:04:00 PM

Pattern: Clear

Page 30: [7] Formatted kate 5/24/22 5:04:00 PM

Pattern: Clear

Page 32: [8] Deleted kate 5/24/22 5:04:00 PM

▼

Page 34: [9] Deleted kate 5/24/22 5:04:00 PM

▼

Page 34: [10] Deleted kate 5/24/22 5:04:00 PM

▼